Eur Biophys J (2012) 41:217–239
DOI 10.1007/s00249-011-0778-0

ORIGINAL PAPER

EBSA
Biophysics in Europe

Cooperative lattice dynamics and anomalous fluctuations of microtubules

Hervé Mohrbach · Albert Johner · Igor M. Kulić

Received: 31 August 2011 / Revised: 19 November 2011 / Accepted: 22 November 2011 / Published online: 16 December 2011

Abstract Microtubules have been in the focus of biophysical research for several decades. However, the confusing and mutually contradictory results regarding their elasticity and fluctuations have cast doubt on their present understanding. In this paper, we present the empirical evidence for the existence of discrete guanosine diphosphate (GDP)–tubulin fluctuations between a curved and a straight configuration at room temperature as well as for conformational tubulin cooperativity. Guided by a number of experimental findings, we build the case for a novel microtubule model, with the principal result that microtubules can spontaneously form micron-sized cooperative helical states with unique elastic and dynamic features. The polymorphic dynamics of the microtubule lattice resulting from the tubulin bistability quantitatively explains several experimental puzzles, including anomalous scaling of dynamic fluctuations of grafted microtubules, their apparent length–stiffness relation, and their remarkable curved–helical appearance in general. We point out that the multistability and cooperative switching of tubulin dimers could participate in important cellular processes, and could in particular lead to efficient mechanochemical signaling along single microtubules.

Keywords Microtubules · Allostery · Signaling · Cell mechanics · Cytoskeleton · Biopolymers

H. Mohrbach
Groupe BioPhysStat, Université Paul Verlaine-Metz,
57078 Metz, France

H. Mohrbach · A. Johner · I. M. Kulić (✉)
CNRS, Institut Charles Sadron, 23 rue du Loess BP 84047,
67034 Strasbourg, France
e-mail: kulic@unistra.fr

Introduction

Microtubules (MTs) are fascinating biological macromolecules that are essential for intracellular trafficking, cell division, and maintenance of cell shape. They display unique elastic and dynamic behavior, inherited by their complex self-assembling nanotube structure. Surprisingly, despite an enormous accumulation of knowledge about their structure, the static and dynamic properties of MTs have challenged all attempts at a fully coherent interpretation. In this paper we develop the line of thought leading towards a new theory that provides a more comprehensive understanding of these properties of MTs. The fundamental result is that stabilized MTs spontaneously form large-scale superhelices of micron-sized pitch and diameter. The MT's superhelical structure turns out to be a consequence of a cooperative interaction between its individual subunits that can sustain several stable curved conformations. Cooperativity of fluctuating internal degrees of freedom in combination with the cylindrical MT symmetry lead to a helical state with very unique characteristics in the world of macromolecules: MTs are helices that are permanently but coherently reshaping, i.e., changing their reference ground-state configuration, due to thermal fluctuations. In particular, when clamped by one end, MTs undergo an unexpected zero-energy motion. As we will see, this could be the key to a consistent interpretation of certain challenging experimental results not captured by the conventional scenarios and models. It is worth remarking that the large majority of experiments probing the above-mentioned properties are in vitro experiments on MTs with stabilizing drugs. We stress this point, as the experimentally prevalent presence of stabilizing agents is not innocent and could modify the properties of MTs. Nevertheless, there are reasons to believe that the theory developed here might be valid also for nontreated MTs.

Before embarking on the road to a "polymorphic MT theory," we first review the conventional understanding of the common MT properties as well as some key experiments which will be our necessary guides towards the model we propose. This paper, which extends and deepens a previous short presentation of the idea of polymorphic MTs (Mohrbach et al. 2010), is composed of two parts. In the first part, we provide conceptual and graphical explanations of the ideas behind the model and investigate consequences of the polymorphic MT model developed herein. We hope that this part is self-consistent and didactic enough that a general reader can grasp the basic underlying ideas. In the second, more technical part, the mathematical model is developed and quantitative results are presented. The details and derivations are left to an extensive appendix.

Short review of what is understood about microtubules

Microtubules are cytoskeletal protein filaments of eukaryotic cells fulfilling different structural and mechanical functions in the cell: MTs act as "cellular bones" strongly influencing the cell shape, constitute the main routes for molecular motor-mediated intracellular cargo transport (Howard 2001; Amos 1991), and perform other important tasks such as stirring the cytoplasm (Kulic et al. 2008). Besides, MTs play a central role in the assembly of the mitotic spindle during cell division and are at the heart of the functioning of cilia and flagella (Alberts et al. 2002). This versatility of MTs in a variety of biological functions mainly relies on their unique high stiffness and on their dynamics of assembly and disassembly. The high rigidity of MTs (similar to hard plastic) is due to their structure, which is known in exquisite detail from three-dimensional (3D) electron microscopy reconstructions (Nogales et al. 1999; Huilin et al. 2002): MTs are hollow tubes whose walls are formed by assembly of a variable number N of parallel protofilaments (PFs). The PFs themselves are built by head-to-tail self-association of the $\alpha\beta$-tubulin heterodimer protein subunit (endowing MTs with a polarity) whose structure has been resolved by electron crystallography (Nogales et al. 1998; Löwel et al. 2001).

In vivo, MTs most commonly appear with 13 PFs (Bouchet-Marquis et al. 2007) (although there are exceptions depending on the cell type), whereas in vitro a variety of structures with PF number ranging from $N = 9$ to 16 were observed (Wade et al. 1990; Chretien 1991). Transitions between different lattice types (mostly with gain or loss of one PF) within a single MT are also frequent (Ray et al. 1993; Chrétien et al. 1992; Chretien 2000). The MT lattice can accommodate these different structures by twisting the PFs around the central MT axis, although this process is energetically costly. The typical lattice twist repeat lengths (pitches) are: $+3.4$, $+25$, and -6 μm for MTs with $N = 12$, 13, and 14 PFs, respectively, with "+" and "−" denoting right and left-handed twists (Wade et al. 1990; Chretien 1991, 2000; Ray et al. 1993; Chrétien et al. 1992). As we will see, the lattice twist is an essential property of the model proposed below. Any deviation from the most frequent, energetically favorable, and thus less twisted configuration $N = 13$ implies an internal prestrain in the MT lattice. The latter stress can locally deform the end portions of the lattice or even destabilize it (Hunyadi 2007).

Another internal prestrain in the MT lattice is believed to be caused by the tubulin subunit, which upon incorporation into the lattice hydrolyzes a bound guanosine triphosphate (GTP) molecule, converting it quickly into a GDP–tubulin form which has the tendency to form a curved state, curling radially away from the axis (Mandelkow et al. 1991; Nogales et al. 2003). The constraint imposed by the MT lattice however maintains the GDP–tubulin dimers in a straight unfavorable state, in turn trapping mechanical prestrain. In this conventional view, MTs are seen as internally prestrained but intrinsically straight Euler beams. The GDP–tubulin prestrain is also believed to trigger rapid depolymerization called the polymerization "catastrophe" (Mitchison 1984). MT stability is regulated either by the presence of a thin layer of as yet unhydrolyzed GTP tubulin dimers at the growing MT end [the so-called GTP-cap model, (Erickson 1992; Janosi et al. 2002)] or by the binding of MT-associated proteins (MAP) or of drugs such as taxol.

What is not understood about microtubules

Mechanical properties of stabilized MTs

The presence of the polymerization dynamics often presents an obstacle to investigation of the mechanical properties of the MT lattice. As previously mentioned, it can be switched off by stabilizing agents such as taxol or MAPs. In the bulk of the available in vitro studies, taxol stabilization has been the experimental method of choice for investigating the elastic properties of MT. It is believed that taxol maintains tubulin dimers in an approximately straight conformation and thus prevents depolymerization (Arnal 1995; Amos 1999; Xiao et al. 2006). However, direct electron microscopy (EM) investigations of single taxol–GDP PFs (Elie-Caille et al. 2007) reveals a more complex and interesting picture. A taxol-stabilized single PF can in fact coexist in several conformational states with comparable free energies: a straight state $\kappa_{\mathrm{PF}}^{\mathrm{st}} \approx 0$ and a weakly curved state with intrinsic curvature $\kappa_{\mathrm{PF}}^{\mathrm{wc}} \approx 1/250\,\mathrm{nm}$ (Fig. 1a). A third,

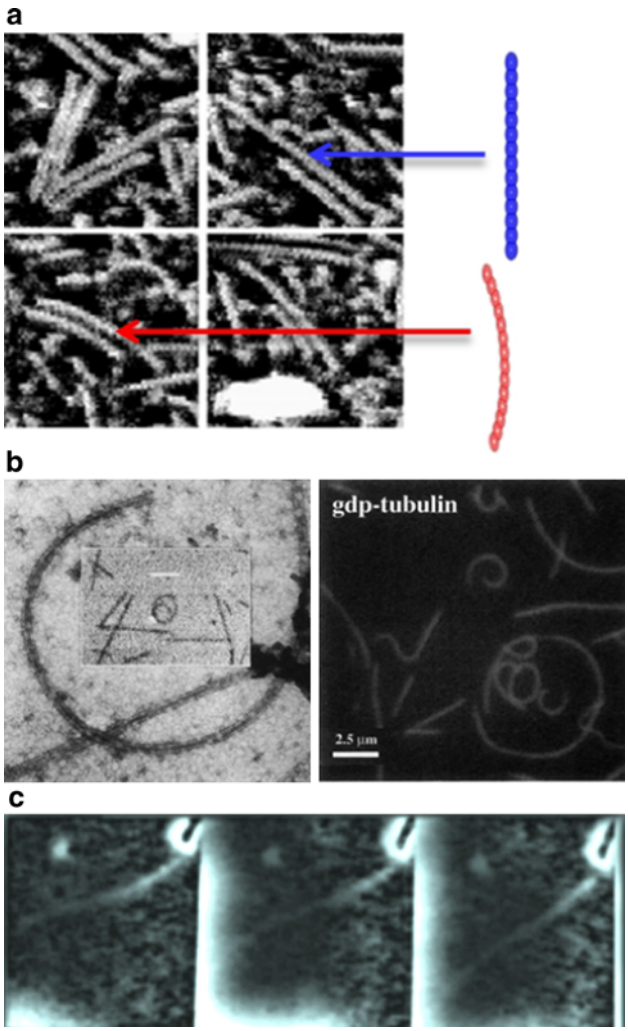

Fig. 1 Empirical evidence for tubulin bistability: **a** A single taxol-stabilized protofilament can coexist in a straight $\kappa_{PF} \approx 0$ and a slightly curved $\kappa_{PF} \approx 1/250\,\text{nm}$ state (reproduction from Elie-Caille et al. 2007); **b** Taxol-stabilized microtubules in gliding assay experiments can switch to a stable circular state and move on circular tracks (from Amos 1991; Vale et al. 1994). Microtubules are occasionally observed to switch back and forth between the circular and straight states. **c** Taxol-stabilized microtubules form a three-dimensional helicoid structure with 15 μm pitch (from Venier et al. 1994)

highly curved state with $\kappa_{PF}^{hc} \approx 1/20\,\text{nm}$ additionally appears after longer observation periods. Notably, Elie-Caille et al. (2007) pointed out a cooperative nature of the straight to curved transition within single PFs. These important findings of several conformational tubulin dimer states and cooperative interaction between them will form a central ingredient of our model below.

Going from a single protofilament to the whole tube, a central mechanical property of interest often measured for stabilized MTs is the persistence length, defined as $l_p = B/k_BT$. Here $B \propto Y$ stands for the flexural rigidity, which for an isotropic beam is proportional to its elastic Young's modulus Y. Several experimental approaches have been developed to measure the bending stiffness of taxol-stabilized MTs. One method consists in measuring the thermal shape fluctuations of MTs via dark-field microscopy (Gittes et al. 1993; Venier et al. 1994) or fluorescence light microscopy (Mickey and Howard 1995). Alternatively in several other experiments, l_p has been determined by applying controlled bending forces via hydrodynamics (Venier et al. 1994), optical tweezers (Felgner et al. 1996; Kikumoto et al. 2006; Kurachi et al. 1995; Takasone et al. 2002), and atomic force microscopy tips (Kis et al. 2002). Interestingly, Gittes et al. (1993) observed that stabilized MTs are not perfectly straight but rather contain some form of quenched curvature disorder which needs to be subtracted from the measurements. In the same vein, dark-field imaging of the thermal fluctuations of the free end of axoneme-bound MTs shows that taxol-stabilized MTs adopt a three-dimensional helicoid structure (Venier et al. 1994) (we return to this point below).

The persistence length obtained from these different experiments is placed in the range 1–8 mm, with some newer studies going down to 0.1 mm (cf. below). For a standard semiflexible polymer (such as actin or DNA) we expect l_p to be a material constant, in particular being independent of the filament length. However, for MTs, the experimental l_p data are not only highly scattered but extremely confusing on this point. That the persistence length could indeed depend on the MT length was first mentioned and observed by Kurachi et al. (1995) and Takasone et al. (2002) and confirmed by other experimental measurements probing either the thermal movement (Vanden Heuvel et al. 2007) or the active bending deformations by electrical fields of individual taxol-stabilized MTs gliding on a kinesin-coated surface (Vanden Heuvel et al. 2008; Kim et al. 2008). In particular, these techniques gave, for short MT segments with submicron length, persistence lengths between 0.08 and 0.24 mm.

This intriguing "length-dependent stiffness" was also investigated by Pampaloni et al., who measured the lateral fluctuations of MTs grafted to a substrate (Pampaloni et al. 2006). These authors found a l_p falling within the range 0.11–5.04 mm for MT lengths varying from 2.6 to 47.5 μm, with a strong linear correlation between length and l_p. A similar experiment done by Taute et al. (2008) measured the longest relaxation time $\tau_{max}(L)$ of MTs of various lengths L. It was found that MTs exhibited unusually slow thermal dynamics compatible with $\tau_{max} \propto L^3$ (cf. Fig. 9), in sharp contrast to standard semiflexible filaments with $\tau_{max} \propto L^4$. Brangwynne et al. (2007) reported that the relaxation time for long MTs ($L > 10$ μm) extracted from two-dimensional (2D) shape analysis of taxol-stabilized fluorescent MTs shows an anomalous dynamics on short scales as well. Furthermore,

it has also been experimentally found that the rigidity of MTs depends on their growth velocity (Janson 2004). All these experiments measuring the bending stiffness and the bending dynamics led the community to the conclusion that the "beam of life" cannot be seen as a simple Euler beam. Its complex internal structure should determine its elastic and dynamical properties. However, which internal mode contributes to the now obvious elastic complexity is the important question, a convincing answer for which is still lacking.

Helices and rings

Even more intriguing than the issue of MT elasticity is perhaps the question: What is the ground state of a MT? While the naive answer—a straight rod—would be the most accepted view, a number of experiments put this mundane, simplistic picture in doubt; for instance, wavy sinusoidal and circular shapes are frequently observed when MTs are adsorbed to glass surfaces or confined between them. In this confined case, Fourier mode analysis of MT deformations systematically reveals that a few discrete modes have larger amplitude than the fluctuations around them (Gittes et al. 1993; Brangwynne et al. 2007; Janson 2004; cf. also Vanden Heuvel et al. 2007, supplementary material). This is a strong hint of the presence of some type of "frozen-in" curvature, dynamically quenched on experimental time scales. Likewise in motility assays, it is often seen that, when MTs glide over a surface coated with molecular motors, they follow wavy sinusoidal and often circular tracks (Amos 1991; Vale et al. 1994) (cf. Fig. 1b). In this context, particularly interesting is the observation by Amos and Amos (1991) of the formation of permanently circling MTs (see Fig. 1b). These unusual stable circular gliding structures persisted for many cycles and occasionally straightened again. As written by Amos (1991), this suggests that "an intact tubular polymer is capable of holding more than one conformational state without the help of an external force." From EM images it was inferred that the underlying mechanism stems from the balance of individual taxol–GDP–tubulin dimers between two or more different stable conformations (Amos 1991).

An even clearer hint towards the real nature of the frozen-in curvature was, as already mentioned, discovered by Venier et al. (1994) (Fig. 1c), who described stabilized MTs as "wavy periodic shapes" with half-period of about 7–8 μm. This observation, combined with the fact that MTs often went out of focus, led the authors to "suggest that taxol-treated microtubules may adopt a three-dimensional helicoid structure of 15 μm pitch."

Therefore, it seems that the MT curvature is a persistent attribute attached to its lattice. Any serious attempt to fully understand the complexity of MT elasticity cannot avoid the question of its ground state. Indeed, understanding fluctuations around a particular state will be futile as long as the origin of the state itself remains obscure.

The soft shear model

A first theoretical attempt to cope with some aspects of the described MT mechanical complexity was the "soft shear model" (also called the "Timoshenko beam model" or "anisotropic composite material model") (Kis et al. 2002; Pampaloni et al. 2006; Heussinger et al. 2007; Mohrbach 2007). In this model the MT is considered as an anisotropic fiber-reinforced material (Kis et al. 2002; Pampaloni et al. 2006) with the tubulin protofilaments acting as strong fibers weakly linked with easily shearable interprotofilament bonds. Some specific equilibrium statistical and mechanical properties of this model were investigated by Heussinger et al. (2007) and Mohrbach (2007). An interesting peculiarity and inherent consequence of this model is that any local lattice deformation gives rise to a long-distance curvature relaxation (Mohrbach 2007) and can lead to a long-range interaction along the MT contour. This aspect of the soft shear model (SSM) is in phenomenological agreement with cooperative deformations induced by enzymes such as katanin. Furthermore, this model predicts a length-dependent persistence length which approximately resembles the measured behavior (Pampaloni et al. 2006; Taute et al. 2008). However, in detail it suffers from a number of difficulties and inconsistencies, in particular:

- The ground state of the SSM is straight, in conflict with the observation of a helical ground state (Venier et al. 1994).
- The SSM does not allow for lattice multistability as observed by Amos and Amos (1991).
- The predicted value of the shear modulus is extremely small (Pampaloni et al. 2006; Taute et al. 2008; Mohrbach 2007) (10^5 to 10^6 times smaller than the Young's modulus). This would imply very strong shearing in bent microtubule structures. This however is unsupported by other experimental evidence. Indeed, observations of straight and highly bent MTs show that bending does not significantly modify the relative position of the interprotofilament bonds (Chrétien et al. 1998).
- The dynamics of clamped MTs (Pampaloni et al. 2006; Taute et al. 2008) does not emerge naturally from the SSM. To reach agreement and fit the experimental dynamics, the shear model needs to introduce an ad hoc internal dissipation of unclear origin.

- For short MTs (<4 μm) that model is very far off and disagrees with the "plateau" region of the bending stiffness versus length relations (cf. Fig. 3 in Taute et al. 2008).

Careful reanalysis of clamped MT experiments (cf. Figs. 2, 3 in Pampaloni et al. 2006; Taute et al. 2008) reveals two features not captured by the SSM: the persistence length scales for large L approximately as $\sim L$ (without signs of saturation) while the relaxation times scale as $\sim L^3$. This exotic behavior naively suggests the presence of a limited angular hinge at the MT clamping point. On the other hand, artifacts that could trivially lead to a "hinged behavior" (such as loose MT attachment and punctual MT damage) were specifically excluded by experiments (Pampaloni et al. 2006; Taute et al. 2008).

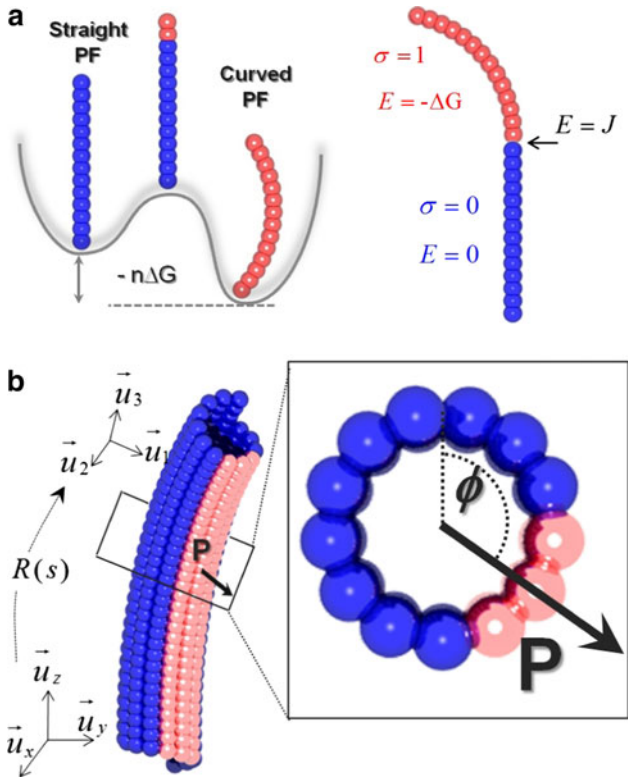

Fig. 2 Elements of the "polymorphic tube model." **a** The GDP–tubulin protofilaments can fluctuate cooperatively between two discrete states. The curved, $\sigma = 1$ state is energetically preferred over the straight, $\sigma = 0$ state with an energy gain $E = -\Delta G$. A junction between straight and curved states along the same protofilament is penalized by a coupling constant $E = +J$. **b** Competition between tubulin switching energy and elastic lattice strain energy leads to spontaneous symmetry breaking: MT bends to a randomly chosen direction and assumes a nonzero polymorphic order parameter P. The energy becomes invariant with respect to an arbitrary rotation of the polymorphic phase angle ϕ

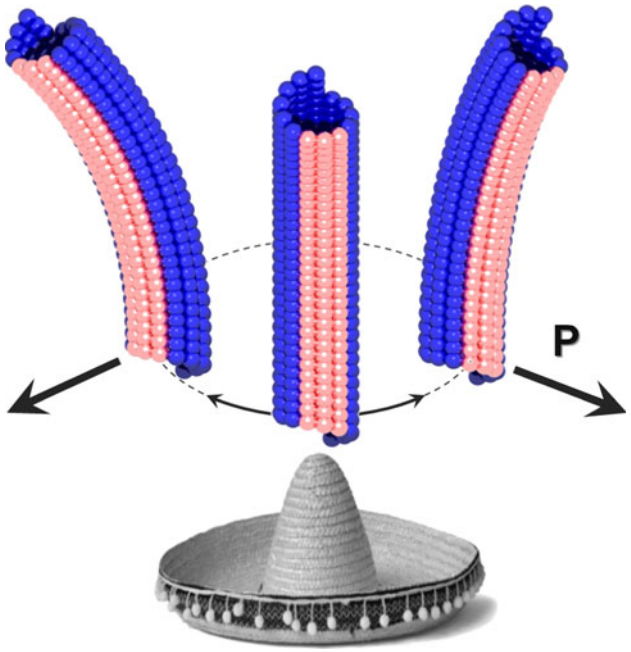

Fig. 3 The straight state of the microtubule becomes unstable and forms a spontaneous bend with fixed curvature pointing towards a randomly chosen direction. The microtubule can assume one of the N degenerate ground states and switches between them at no energy cost; the effective potential has a shape reminiscent of a Mexican hat

Considering all these obstacles, it becomes increasingly clear that the solution to all the puzzles requires a new and radically different hypothesis.

Idea of polymorphic microtubule dynamics

The new scenario proposed here is based on the hypothesis of *cooperative internal* MT lattice dynamics. The two central assumptions of our model are as follows:

(I) The taxol–GDP–tubulin dimer is a conformationally multistable entity and fluctuates between at least two states on experimental time scales: a straight and an outwards curved state (Figs. 1a, 2a).

(II) There is a nearest-neighbor cooperative interaction of tubulin states along the PF axis.

Note that assumption I is very different from the conventional picture where GDP–tubulin has only *one* energetically favorable (curved) state. We will show that a model based on assumptions I and II straightforwardly leads us to the very origin of MT (super)helicity and provides a coherent explanation for static and dynamic measurements in thermal fluctuation experiments.

In contrast to the soft shear model, the present model is elastically isotropic but the monomer curvature is bistable. As we will see, the ground state in this new model is a

highly degenerate, three-dimensional helix fluctuating between many equivalent configurations.

Conformational symmetry breaking and helix formation

In this section we provide a simple pictorial panorama of the consequences of assumptions I and II. What happens when tubulin dimers obeying assumption I are trapped in the circularly symmetric MT lattice? Starting from assumption I we imagine that the straight and curved GDP–tubulin states have a certain energy difference $\Delta G > 0$, with the curved state being slightly more favorable. The strict preference for the curved state is however only true if the tubulin dimers are free, i.e., not confined to the lattice. The situation becomes more interesting once they are incorporated into the lattice. Obviously the outwards bending tendency of the curved state is in conflict with the geometry of the lattice. Switching a dimer on one MT side will frustrate the dimers on the opposite side of the tube and prevent them from switching at the same time. On the other hand, the direct neighbors of the curved dimer (on the same MT side) will profit and switch more easily to the curved state, as the lattice is already slightly "prebent" in the correct direction. This peculiar interplay of negative and positive interactions gives rise to a clustering of curved dimer states into a single block on one side of the tube (cf. Fig. 2b).

This immediately raises the question of the orientation of this curved dimer block. Which MT side will be selected, and in which direction will the MT overall bend, can only be decided by the process of *spontaneous symmetry breaking*; that is, if the ground state is a curved dimer block, it will be a highly degenerate state (see Fig. 3). In turn, it can be expected to move through the lattice thermally at nearly no energy cost (apart from some friction). This is the most essential feature of the present model.

So far we have considered only a single MT cross-section. If assumption II (cooperativity) were not to hold, the curved state blocks would pick their sides at each section completely independently. The tube would locally curve in random uncorrelated directions, and the effect of tubulin multistability would remain essentially invisible at larger scale. However, according to assumption II, the blocks become correlated in orientation and prefer to stack on top of each other. Macroscopically, this would then lead to a bent—in fact circular—MT if the PF were not twisted around the central MT axis (see Fig. 2b). This provision brings us to the final interesting point. As already mentioned, MT lattices are generically twisted; i.e., their PFs are not strictly parallel. With a cooperative interaction along the PFs—which are now twisting around the tube axis—the final product of assumption I and II will be a long-pitched helix. The pitch of the helix should coincide with the lattice twist repeat length: +3.4, +25, and −6 μm for MTs with $N = 12$, 13, and 14 PFs, respectively. The created "polymorphic helix," however will not be unique and will be able to reshape between its N indistinguishable orientation states.

When we graft one end of such a polymorphic helix onto a surface [as, e.g., performed by Pampaloni et al. (2006) and Taute et al. (2008], the helix will still be able to switch between the equivalent orientations and perform a motion that we call "wobbling" (see Fig. 4). It is exactly this type of motion that can give rise to the static and dynamic effects measured by Pampaloni et al. (2006) and Taute et al. (2008).

To see this, we can approximate the movement of a clamped polymorphic helix that is switching between its equivalent ground states with a "rigid conical rotor" (see Fig. 4). For such a rotor the transverse displacement ρ of the MT end grows linearly with its length L. Using the naive definition of persistence length $l_p \approx L^3/3\langle\rho^2\rangle$ (where $\langle\rangle$ is the ensemble average) and the fact that $\langle\rho^2\rangle \propto L^2$, this apparent persistence length becomes proportional to the length, i.e., $l_p \propto L$. This scaling (cf. Fig. 11) is in agreement with the experimental results of Pampaloni et al. (2006) and Taute et al. (2008), giving us the first hint that the model is on the right track. Appendix E comments on the robustness of this conical hinge-like motion against limited local hindrance of the wobbling mode due to the adsorbed part of the grafted MT.

Further encouragement comes from study of the dynamics of the model. Making again the approximation of a rigid conical rotation (induced by wobbling) the observed

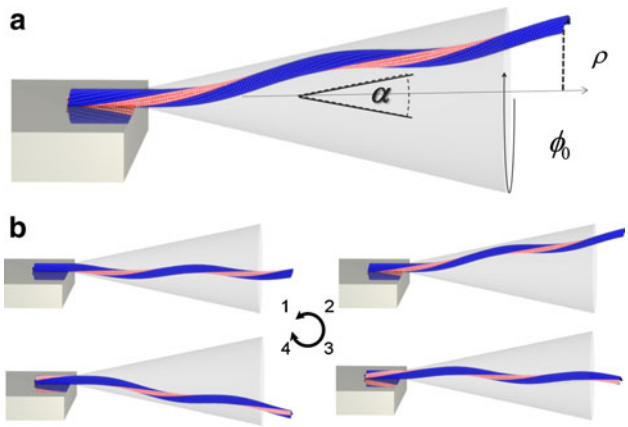

Fig. 4 A clamped polymorphic microtubule with intrinsic lattice twist attached at its end to a substrate (Pampaloni et al. 2006; Taute et al. 2008) performs a peculiar movement. It forms a polymorphic helix with N degenerate ground states and switches between them at no energy cost. The approximately conical motion with opening angle α leads to anomalous lateral fluctuations $\langle\rho^2\rangle \sim \alpha^2 L^2$, radically different from all other semiflexible filaments

unusual scaling of the longest relaxation time $\tau_{max} \propto L^3$ can also be easily understood. In fact, a slender object of length L rotated along a conical surface has a friction constant $\xi_{rot} \propto L^3$. In turn, the longest relaxation time is given by the diffusional equilibration time on the cone, i.e., $\tau_{max} \propto \xi_{rot}/k_B T \propto L^3$ (cf. Fig. 12). It turns out that the model correctly predicts both the exponent and the prefactor of the experimental relaxation time.

In addition, it is further reassuring that the helical ground state(s) of the model provides a rationale for the observation of MT helices by Venier et al. (1994).

In vivo implications of microtubule polymorphism

The bulk of observations cited herein were made in vitro on taxol-stabilized MTs. It is known that taxol inhibits MT disassembly by maintaining the tubulin dimer in a state that strongly favors polymerization. However, from the experiments reported above it is also clear that taxol does not suppress all tubulin conformational changes: the taxol–GDP–tubulin dimer has multiple stable conformations (Elie-Caille et al. 2007). How do these in vitro findings relate to MTs in vivo?

It is a common empirical observation in many in vivo systems that, despite their high bending stiffness, MTs are often seen curved or highly wavy on micron scales (Bicek et al. 2009; Brangwynne et al. 2006, 2007 ; Keating et al. 1997; Kaech et al. 1996; Samsonov et al. 2004); for instance, in Bicek et al. (2009), highly sinusoidal MTs on the periphery of living LLC-PK1 cells were observed. These shapes are usually explained as a consequence of motor-induced buckling opposed by a gel-like environment that leads to finite-wavelength buckling (Brangwynne et al. 2006). While this "buckling in a gel" interpretation is physically appealing, a closer look at the data in Brangwynne et al. (2006) (in particular the accompanying movie material) reveals an absence of correlation in buckling *directions* of neighboring MTs. This observation puts a question mark over the participation of a background continuum gel, as in this case the strains in the gel would necessarily propagate to neighboring microtubules and lead to spatially correlated buckling events, in sharp contrast with observations. Therefore, we are left with a robust phenomenon of sinusoid, constant-wavelength MTs, but without a definite interpretation so far.

The phenomenology of stable rings (Amos 1991) and wavy sinusoidal MTs forming in gliding assays (Vale et al. 1994) is strikingly similar and visually indistinguishable from the pure in vivo observations (Bicek et al. 2009; Brangwynne et al. 2006, 2007; Keating et al. 1997; Kaech et al. 1996; Samsonov et al. 2004). Indeed, in both situations highly curved lattice states of very similar magnitudes $\kappa_{MT} \approx 1 - 2\,\mu m^{-1}$ are readily observed. This analogy between in vivo and in vitro cases suggests that tubulin dimers, both in vivo and taxol stabilized (in vitro), possess an identical highly curved state ($\kappa_{PF}^{hc} \approx 1/20\,nm$). This highly curved state appears to be activated within the lattice only under compressive loads and seems to be a universal property of GDP–tubulin itself, independent of taxol stabilization.

On the other hand, the weakly curved state of taxol–GDP-dimer ($\kappa_{PF}^{wc} \approx 1/300\,nm$) is soft enough to be activated by thermal fluctuations. The empirical evidence for the weakly curved state in vivo is far less obvious than for the highly curved state. The slight deformations induced by the former would be more difficult to distinguish from other MT-deforming effects in living cells such as motors, polymerization forces, presence of lattice defects, bundling, and microtubule-associated protein action. However, the observed phenomenology of length-dependent persistence length of MTs growing from centrosomes in egg extracts (Keller et al. 2008) (no taxol present) qualitatively and quantitatively resembles the in vitro observations (Pampaloni et al. 2006; Taute et al. 2008). This is one more indication that the dynamic MT polymorphism could persist also in vivo.

At least two possible biological implications of the helicoidal polymorphic MT nature come immediately to mind. First, a curved or helical beam under compressive load responds like a mechanical spring and is therefore much softer (in tension, compression, and bending) than a straight beam. Therefore, a network of helical MTs might be important for the overall mechanical compliance of the cell. A perfectly straight MT buckled by an extracellular load would be much more susceptible to mechanical failure and depolymerization than a soft, compliant helix. Second, helical shapes are geometrically (topologically) prevented from side-by-side aggregation and can thus evade formation of bundles, instead forming loose networks with many fewer contacts. It appears that a tuned helicity (that can be switched on or off) could be a good mechanical control parameter for the formation of different cytoskeletal structures. While the bulk of the cytoplasmic MTs are preferably in the loose network state (favored by helicity), in occasional situations such as in neuronal axons, straight aligned MTs are required. In such a situation, bundling could be triggered by switching the lattice to the straight state. Remarkably, in the process of axonal retraction, the straight axonal bundle is destabilized (and eventually contracts towards the cell soma) by an apparent transition of the MTs to a wavy coiled state (Fridoon et al. 2000) very reminiscent in shape to single wavy MTs from cell soma (Bicek et al. 2009; Brangwynne et al. 2006, 2007; Keating et al. 1997; Kaech et al. 1996; Samsonov et al. 2004).

In general, MT polymorphism might have other, less obvious biological implications that still have to be identified. In particular, a more speculative possibility is that tubulin's allosteric multistability might also be a piece in the puzzle of MT "catastrophes." A cooperative curvature switch might trigger a transition from growth to depolymerization. Maybe the most fascinating aspect could lie in the possibility of signal transmission along single MTs via a long-range conformational switch. If our model is correct, this is the most inherent and distinct consequence of the underlying mechanism.

This concludes the qualitative description of the essential ideas behind the polymorphic tube model. In the following we switch gears and present in more quantitative detail the mathematical model. The mathematically less inclined reader is invited to browse through the figures and comparisons with experiments, maybe pick up additional concepts (such as polymorphic defects and their dynamics), and jump to the "Perspectives" section, which underlines the essential biological consequences.

The polymorphic tube model

Until now the discussion has been qualitative, whereas in the following we build the mathematical model of the polymorphic MT. We will provide quantitative arguments and model experimental data, thus justifying a posteriori the previous discussion. In this section, we focus on the thermally induced weakly curved state in taxol-stabilized MTs, leaving the case of mechanically induced highly curved MTs for further work.

We model the GDP–tubulin dimer state by a two-state variable $\sigma_n(s) = 0,\ 1$ corresponding to the straight and curved state at each lattice site. $n = 1, \ldots, N$ is the circumferential PF index, and $s \in [0,\ L]$ is the longitudinal position variable along the MT centerline. We recall that our model is based on the following assumptions:

(I) The taxol–GDP–tubulin dimer fluctuates between two states—straight and curved (Fig. 2a)—with an energy difference $\Delta G > 0$ favoring the curved state. The energy density resulting from the switching of tubulin dimers (at a given MT section) is then given by

$$e_{\text{trans}}(s) = -\frac{\Delta G}{b}\sum_{n=1}^{N}\sigma_n(s) \tag{1}$$

with $b \approx 8\,\text{nm}$ being the dimer length.

(II) There is an Ising-type nearest-neighbor cooperative interaction of tubulin states *along* the PF axis with an interaction energy $J > 0$ favoring nearest-neighbor dimers on the same PF to be in the same state. This leads to the interaction energy density

$$e_{\text{inter}}(s) = -\frac{J}{b}\sum_{n=1}^{N}(2\sigma_n(s)-1)(2\sigma_n(s+b)-1). \tag{2}$$

The final term required for our description is the elastic energy density of the MT lattice. For a usual isotropic Euler beam the material deformations ε are related to the centerline curvature vector $\vec{\kappa}$ via $\varepsilon = -\vec{\kappa}\cdot\vec{r}$ with $\vec{r}$ the radial material vector in the cross-section. For a polymorphic MT, modeled as a continuum material made of N PFs ($N = 11$–16), its actual deformation will depend on the polymorphism-induced prestrain ε_{pol}. In this case the elastic energy density of the MT can be written as

$$e_{\text{el}}(s) = \frac{Y}{2}\int_{R_\text{i}}^{R_\text{o}}\int_{0}^{2\pi}\left(\varepsilon-\varepsilon_{\text{pol}}\right)^2 r\,\mathrm{d}r\mathrm{d}\alpha, \tag{3}$$

where the integration in e_{el} goes over the annular MT cross-section with $R_\text{i} \approx 7.5\,\text{nm}$ and $R_\text{o} \approx 11.5\,\text{nm}$ being the inner and outer MT radii, respectively. The prestrain ε_{pol} is a function of the polymorphic state of the tubulin dimers. Its definition requires a decomposition of the tubulin dimer into an inner part (facing the tube axis) and an outer part (facing outwards from the tube axis) (cf. Fig. 5). We assume that each curved dimer state generates a positive prestrain $+\varepsilon_{\text{PF}}$ on its inner part and an equal but negative prestrain $-\varepsilon_{\text{PF}}$ on its outer part. We can then write $\varepsilon_{\text{pol}}(s,r,\alpha) = \varepsilon_{\text{PF}}\sigma_n(s)\left[I_{[R_\text{i},R_\text{o}-d_{\text{PF}}/2]}(r) - I_{[R_\text{o}-d_{\text{PF}}/2,R_\text{o}]}(r)\right]\cdot I_{\left[\frac{2\pi}{N}n+q_0 s,\frac{2\pi}{N}(n+1)+q_0 s\right]}(\alpha)$, where $I_{[\cdot]}(x) = 1$ if $x \in [\cdot]$ and 0 otherwise (Heaviside function) and d_{PF} is the PF diameter. The parameter q_0 appearing in the angular part of ε_{pol} is the natural lattice twist that leads to the proper geometric rotation of a PF around the tube axis. This parameter is lattice type dependent and takes discrete values $2\pi/q_0 = +3.4\ \mu\text{m}$, $+25\ \mu\text{m}$, and $-6\ \mu\text{m}$ for MTs with $N = 12$, 13, and 14 PFs, respectively (Wade et al. 1990; Chretien 1991, 2000; Ray et al. 1993). We can estimate the prestrain ε_{PF} from the experimental value of the single

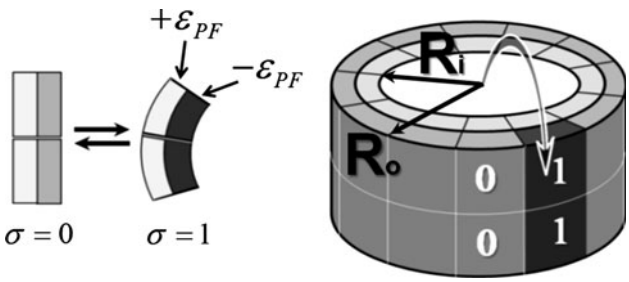

Fig. 5 Strains and deformations in the polymorphic tube model. Each tubulin dimer can fluctuate between a straight, $\sigma = 0$ state and a curved, $\sigma = 1$ state with intrinsic curvature κ_{PF}. The curved tubulin dimer generates a positive prestrain $+\varepsilon_{\text{PF}}$ on its inner part and an equal but negative prestrain $-\varepsilon_{\text{PF}}$ on its outer part with strains related to observed dimer curvature via $\varepsilon_{\text{PF}} = (R_\text{o} - R_\text{i})\kappa_{\text{PF}}/2$

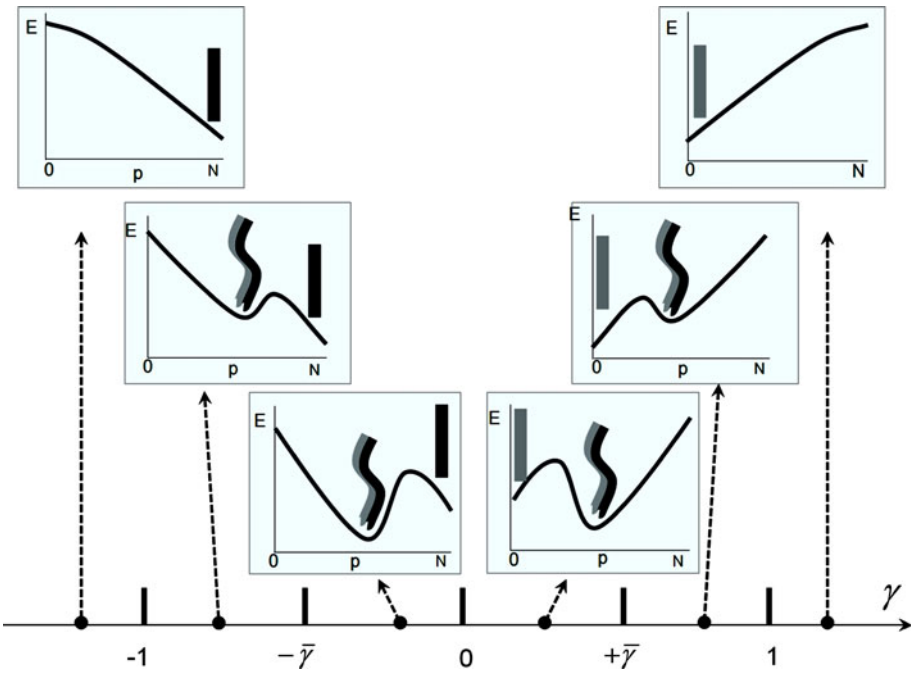

Fig. 6 Phase diagram of the polymorphic microtubule model as a function of the polymorphic–elastic interaction parameter γ from Eq. 7. Depending on the magnitude and sign of γ the microtubule can be in an "all PF switched state" (*black*), "no PF switched state" (*grey*), or mixed curved–helical state. Only the latter "mixed state" will display net curvature and lead to an observable helical appearance

switched PF's curvature $\kappa_{\mathrm{PF}} \approx (250\,\mathrm{nm})^{-1}$, measured by Elie-Caille et al. (2007) on single taxol-stabilized PFs, to be $\varepsilon_{\mathrm{PF}} = d_{\mathrm{PF}}\kappa_{\mathrm{PF}}/2 \approx 10^{-2}$. Collecting all energy contributions together the total (elastic + polymorphic) energy of the MT is then given by

$$E_{\mathrm{MT}} = \int_0^L (e_{\mathrm{el}} + e_{\mathrm{trans}} + e_{\mathrm{inter}})\mathrm{d}s. \tag{4}$$

The ground state within this model is determined by the interplay of the first two terms e_{el} and e_{trans}. The last term e_{inter} determines the cooperativity and is responsible for the suppression of defects in the ideal polymorphic order (cf. Fig. 7). A large value of the cooperativity constant with $J \gg k_B TL/b$ would imply a defect-free lattice. However, the presence of the latter defects (and their motion) is a necessary ingredient for the overall rearrangement of the helix, as discussed below.

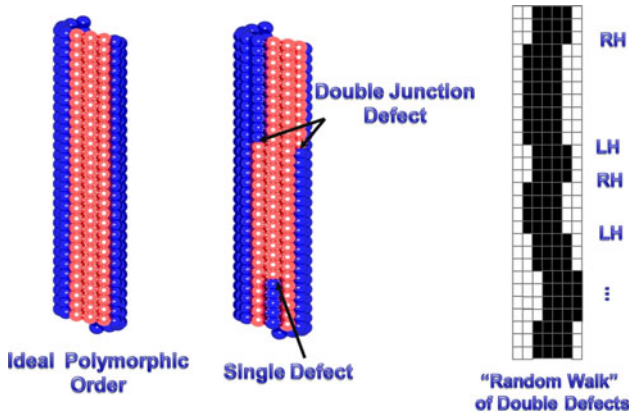

Fig. 7 Defects in ideal polymorphic order soften the helical states and give rise to "polymorphic dynamics." Single defects carry a cost proportional to their length, whereas double defects make only a local energy contribution. The coexistence of left- and right-handed defects (LH and RH) along the length leads to a "random walk" of the polymorphic curvature direction and in turn to an effective torsional deformation

To understand the basic behavior of the ideal helical ground state without defects, i.e., where PFs are individually in a uniform state (either curved or straight), we initially restrict ourselves to the simplified energy density $e = e_{\mathrm{el}} + e_{\mathrm{trans}}$. To investigate the MT geometry we first introduce two reference frames (Fig. 2b). One is the material frame with base vectors $(\vec{u}_1, \vec{u}_2, \vec{u}_3)$ attached to the MT cross-section. The other is an external fixed laboratory frame with base vectors $(\vec{u}_x, \vec{u}_y, \vec{u}_z)$. Putting the MT along the $\vec{u}_z$ axis direction and considering small MT angular deflections we have $\vec{u}_z \approx \vec{u}_3$. In this case the two frames are simply related to each other by a rotation transformation $R(s)$ given by the internal MT lattice twist q_0, such that $(\vec{u}_x, \vec{u}_y) = R(s)(\vec{u}_1, \vec{u}_2)$ with

$$R(s) = \begin{pmatrix} \cos q_0 s & -\sin q_0 s \\ \sin q_0 s & \cos q_0 s \end{pmatrix}. \tag{5}$$

To rewrite e in a more illuminating fashion, we define two important order parameters at each MT cross-section. The first is the *vectorial polymorphic order parameter*

$$\vec{P}(s) = \sum_{n=1}^{N} \left(\vec{u}_1 \cos\frac{2\pi n}{N} + \vec{u}_2 \sin\frac{2\pi n}{N} \right) \sigma_n(s).$$

Physically, $\vec{P}$, a 2D vector at each local material frame section attached to the MT (cf. Fig. 2b), describes the asymmetry of distribution (a kind of "polarization") of the dimer states. It acquires a nonzero value only in the case when the curved and noncurved states are azimuthally separated on opposite MT sides; for instance, the "all-straight" or "all-curved" PF state both correspond to the same value $\vec{P} = 0$. Besides the vector $\vec{P}$, we need to define a second (scalar) quantity

$$M(s) = \sum_{n=1}^{N} \sigma_n(s),$$

which counts the total number of dimers in the curved state at cross-section s (or in the Ising model terminology, the "magnetization"). After integration of Eq. 3 over the cross-section and some algebra, the energy density $e = e_{\mathrm{el}} + e_{\mathrm{trans}}$ can be written in the more appealing form

$$e = \frac{B}{2}\left[\left(\vec{\kappa} - \vec{\kappa}_{\mathrm{pol}}\right)^2 + \kappa_1^2 \left(\frac{\pi}{N}\gamma M - \sin^2(\pi/N)\vec{P}^2 \right) \right] \tag{6}$$

with the elastic bending modulus $B = \frac{\gamma\pi}{4}\left(R_{\mathrm{o}}^4 - R_{\mathrm{i}}^4\right)$, with $\kappa_1 = \frac{(R_0 - R_1)^2}{\pi\left(R_{\mathrm{o}}^2 + R_{\mathrm{i}}^2\right)}\kappa_{\mathrm{PF}}$ and a dimensionless parameter

$$\gamma = \frac{\kappa_{\mathrm{PF}}}{\kappa_1} - \frac{2N\Delta G}{bB\kappa_1^2}. \tag{7}$$

For small deviations of the tube axis from the $\vec{u}_z$ direction, the polymorphic curvature vector $\vec{\kappa}_{\mathrm{pol}}$ in the external coordinate frame $\left(\vec{u}_x, \vec{u}_y\right)$ is related to $\vec{P}$ (in the internal frame $(\vec{u}_1, \vec{u}_2)$) via the transformation in Eq. 5 as

$$\vec{\kappa}_{\mathrm{pol}} = cR(s)\vec{P} \tag{8}$$

with $c = \sin(\pi/N)\kappa_1$, a geometric proportionality constant.

Phase diagram

In the absence of defects, the energy expression (Eq. 6) allows one to determine the conformational ground state of a polymorphic MT. To this end, we first resort to one further small simplification and make the "single block ansatz"; i.e., at each cross-section we assume only a single continuous block of p switched PFs. This ansatz was previously used by Calladine and has been proven very useful in modeling bacterial flagellin polymorphic states (Asakur 1970; Calladin 1975). In the ground-state configuration the curvature is given by $\vec{\kappa} = \vec{\kappa}_{\mathrm{pol}}(p)$, whose absolute value obtained from Eq. 8 is $\kappa_{\mathrm{pol}}(p) = \kappa_1 \sin(\pi p/N)$. The optimal switched block size $p = p^*$ can be determined by minimizing the second term in Eq. 6, which within this ansatz becomes

$$e = \frac{B\kappa_1^2}{2}\left(\gamma\frac{\pi}{N}p - \sin^2\left(\frac{\pi}{N}p\right) \right). \tag{9}$$

This gives rise to an interesting MT phase behavior (cf. Fig. 6). The latter only depends on the polymorphic–elastic competition parameter γ from Eq. 7, which measures the ratio between the polymorphic energy of tubulin switching and the purely elastic cost of this transition.

For $\gamma < -1$ the chemical switching potential ΔG strongly dominates the elastic energy cost $bB\kappa_1^2$. Therefore, switching is highly favorable and all the PFs will be found in the $\sigma = 1$ state. This gives rise to a straight but highly prestrained configuration.

Analogously for $\gamma > 1$, the bending energy contribution is too costly for PFs to switch at all. Therefore, in this regime the PFs are all in the straight state with $\sigma = 0$ and the MT is consequently straight as well.

For $-1 < \gamma < 1$ the situation is more interesting. In this interval we have a coexistence of two locally (meta) stable MT conformations: the straight tube (prestressed or not, depending on the sign of γ) and a curved lattice state with p^* switched protofilaments. For $-\overline{\gamma} < \gamma < \overline{\gamma}$ with $\overline{\gamma} \approx 0.72$, the curved lattice state is the absolute energy minimum and the straight state is only metastable. Therefore, in this regime and in the absence of twist ($q_0 = 0$), the ground-state configuration of the whole tube would be a simple circular arc section (cf. Fig. 2b). On the other hand, the ground state of a microtubule bearing natural lattice twist $q_0 \neq 0$ will be helical (cf. Fig. 4).

It is easy to see that a stable helical state as observed by Venier et al. (1994) is only possible for a switching ratio $p^*/N \in [1/4, 3/4]$. This together with $\kappa_{\mathrm{PF}} = 1/250$ nm (from Elie-Caille et al. 2007) and $\kappa_{\mathrm{pol}}(p^*) = \kappa_1|\sin(\pi p^*/N)|$ provides us with a direct estimate of the radius of curvature $\kappa_{\mathrm{pol}}^{-1} \approx 9 - 14\,\mu\mathrm{m}$. Very strikingly, this range closely reproduces the observed MT helical curvatures as estimated from Venier et al.'s work (1994) $\kappa_{\mathrm{measured}}^{-1} \approx 11\,\mu\mathrm{m}$, lending strong support to the model. Furthermore, taking the helical state stability as an empirical fact (implying that $|\gamma| < 0.72$) and assuming a typical protein Young's modulus of $Y \approx 1 - 10\,\mathrm{GPa}$ enables a simple estimate of the transition energy per monomer as $\Delta G \approx +1.1$ to $+11kT$, a reasonable range for a soft biological object.

In general, the full energy expression, including the cooperativity energy term (Eq. 4), gives rise to a very complex behavior. Here we will focus on some basic new phenomena. It turns out that the most remarkable deviation from standard wormlike chain (WLC) behavior arises from the fluctuation dynamics of the polymorphic order parameter's angular phase, which we consider in the following.

Polymorphic phase fluctuations

Here we introduce a sightly different phenomenological model that simplifies the study of Eq. 4 while still reflecting important aspects and physical properties of it. In this section we assume as before that the helical state is the ground state and consider now the effect of the fluctuations around it. To this end we decompose the polymorphic order parameter as

$$\vec{P}(s) = P(s)[\cos(\phi(s))\vec{u}_1 + \sin(\phi(s))\vec{u}_2],$$

with $P(s)$ being the "polymorphic amplitude" and $\phi(s)$ the "polymorphic phase variable." The latter determines the orientation of the switched block tubulin dimers at each cross-section with respect to the MT material frame. From Eq. 8, the centerline curvature with respect to a fixed external $(\vec{u}_x, \vec{u}_y)$ frame is then

$$\vec{\kappa}_{\mathrm{pol}}(s) = \kappa_0\left[\cos(q_0 s + \phi(s))\vec{u}_x + \sin(q_0 s + \phi(s))\vec{u}_y\right], \tag{10}$$

with $\kappa_0 = cP(s)$.

In general, both the polymorphic phase ϕ and amplitude P can fluctuate along the MT contour and contribute to the polymorphic energy. The phase fluctuations are induced by creation and motion of polymorphic "double defects" (cf. Fig. 7). The double defect, a kind of "polymorphic dislocation" that can be either left or right handed, maintains the number of switched protofilaments constant while reorienting the direction of curvature. At zero temperature the lattice would be defect free, ϕ would be constant, and the polymorphic order parameter $\vec{P}$ would strictly follow the lattice twist. The phase change $\phi' \equiv \mathrm{d}\phi/\mathrm{d}s$ will deviate from zero if on relevant length scales there are enough polymorphic double defects to allow for reorientation of the polymorphic order parameter away from optimum. The double defects carry only a limited local energy cost $\Delta E = 2J$ per defect and can be easily thermally excited if $J \lesssim k_{\mathrm{B}}T$. In the approximation of a large number of PFs, assuming that ϕ can change continuously, we can write the phase contribution to the energy as

$$E_{\mathrm{pol}}(\phi) = \frac{C_\phi}{2}\int_0^L \mathrm{d}s\phi'^2, \tag{11}$$

with the polymorphic phase stiffness $C_\phi \approx k_{\mathrm{B}}T\frac{N^2 b}{8\pi^2}\left(2 + \mathrm{e}^{2J/k_{\mathrm{B}}T}\right)$, which can be related to the density of double defects with energy $2J$ (cf. Fig. 7 and Appendix A), giving rise to a new length scale: the *polymorphic phase coherence length* $l_\phi = C_\phi/k_{\mathrm{B}}T$. For MTs shorter than l_ϕ we will observe coherent helices, while on longer length scales the helix softens significantly and eventually loses its helical appearance.

In contrast to the just discussed polymorphic dislocations which can be easily thermally excited, the variation of the polymorphic amplitude P, i.e., change of the number of switched PFs, is more energetically costly. Any deviation of P from its optimum state P^* (given by the phase diagram) is associated with an energy cost $E \propto (|P| - |P^*|))^2 \cdot l$ proportional to the length l of the region in the unfavorable state (cf. Fig. 7; see Appendix B). Therefore we conclude that, on large enough scales, the polymorphic phase fluctuations will be the dominant effect. Based on this and on the observation of stable helical states (Venier et al. 1994) we will in the following assume $P = \text{const}$.

For small deflections around the z axis, the unit vector tangent to the MT's centerline is approximately given by $\vec{t} \approx (\theta_x, \theta_y, 1)$ in the laboratory frame $(\vec{u}_x, \vec{u}_y, \vec{u}_z)$, where $\vec{\theta} = (\theta_x, \theta_y)$ are the centerline deflection angles in x/y direction. The global centerline curvature $\vec{\kappa} = \mathrm{d}\vec{t}/\mathrm{d}s$ can then be approximated as $\vec{\kappa} \approx \left(\theta_x', \theta_y', 0\right)$, and the total MT energy can be written as follows:

$$E_{\mathrm{tot}} = E_{\mathrm{pol}}(\phi) + E_{\mathrm{el}}(\theta, \phi). \tag{12}$$

The first energy term is the polymorphic phase contribution (Eq. 11). The second term is the elastic bending energy

$$E_{\mathrm{el}}(\theta, \phi) = \frac{B}{2}\int_0^L (\vec{\theta}' - \vec{\kappa}_{\mathrm{pol}})^2 \mathrm{d}s. \tag{13}$$

From Eqs. 11–13, we see that the zero-temperature ground state corresponds to $\phi = \text{const.}$ and $\vec{\theta}' = \vec{\kappa}_{\mathrm{pol}}$, that is, to a defect-free helix with a pitch given by the natural lattice twist q_0. At finite temperature, both elastic and polymorphic fluctuations will be excited so that the curvature can be decomposed as $\vec{\theta}' = \vec{\kappa}_{\mathrm{pol}} + \vec{\theta}'_{\mathrm{el}}$ with $\vec{\theta}'_{\mathrm{el}}$, the purely elastic contribution. This gives rise to a helical MT shape described by the curvature $\vec{\kappa}_{\mathrm{pol}} + \vec{\theta}'_{\mathrm{el}}$ and torsion $\tau \sim \phi' + q_0$. The MT lateral displacements away from the z axis can be written as $\vec{\rho}(s) = (x(s), y(s)) = \int_0^s (\theta_x(s')), \theta_y(s')))\mathrm{d}s'$, which for small deflections decouples into elastic and polymorphic displacements $\vec{\rho}(s) = \vec{\rho}_{\mathrm{pol}} + \vec{\rho}_{\mathrm{el}}$, where $\vec{\rho}_{\mathrm{el}} \approx \int_0^s \vec{\theta}_{\mathrm{el}}(s')\mathrm{d}s'$ and $\vec{\rho}_{\mathrm{pol}} \approx \int_0^s \vec{\theta}_{\mathrm{pol}}(s')\mathrm{d}s'$. The latter can also be written from Eq. 10 as

$$\vec{\rho}_{\mathrm{pol}}(s) = \kappa_0 \int_0^s \mathrm{d}s' \int_0^{s'} \mathrm{d}\tilde{s}\left(\cos(q_0\tilde{s} + \phi(\tilde{s}))\vec{e}_x + \sin(q_0\tilde{s} + \phi(\tilde{s}))\vec{e}_y\right). \tag{14}$$

In Fig. 8, snapshots of configurations of clamped MT obtained from Monte Carlo simulations are plotted for different concentrations of double defects (i.e., different values of l_ϕ) with twist and no twist. It is interesting to remark at this point that, based on the symmetry in the problem, any MT configuration can be rotated around the z axis with no energy cost. This seemingly trivial feature—the energetic degeneracy—is in fact the most distinctive and unusual property of a polymorphic chain. We consider the consequences in the following.

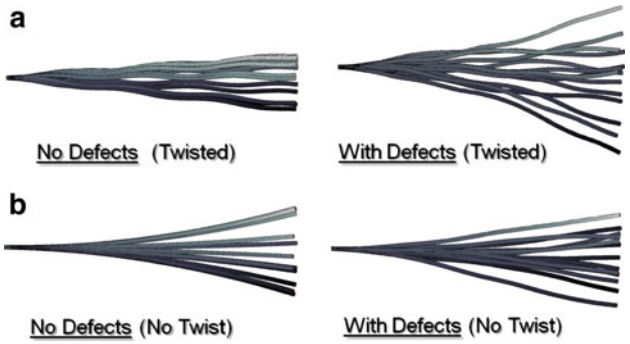

Fig. 8 Conical "wobbling" motion due to the rotational energy degeneracy of the polymorphic MT model: snapshots of Monte Carlo simulated lattice states. **a** Twisted MTs free of defects $L/l_\phi \ll 1$ and with numerous defects $L/l_\phi > 1$. For larger number of defects, the helix looses its coherent appearance. **b** For nontwisted MTs the movement has a typical parabolic "trumpet-like" shape

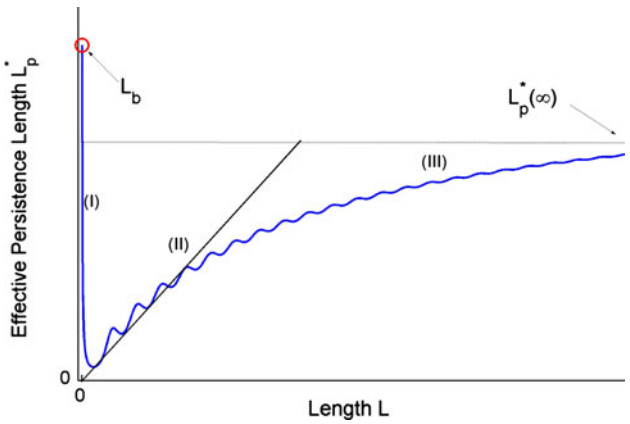

Fig. 9 A typical shape of the effective persistence length $l_p^*(L)$ for a clamped microtubule as obtained from Eqs. 16, 18, and 20. Most generically, the curve displays three different regimes: (I) an initial rapidly decreasing regime where polymorphic effects become more effective with growing L (softening the chain), (II) a linearly growing oscillatory regime corresponding to the coherent wobbling movement of the clamped microtubule, and (III) an asymptotic plateau regime where the helix progressively loses its coherence with growing L. In this regime, the behavior tends to that of a classical semiflexible chain yet with a renormalized effective persistence length given by Eq. 23

The wobbling mode

By construction, a polymorphic chain as we describe it here has a N-fold symmetry. Therefore, there are N different helical states of different orientations with the same energy, i.e., N ground states. This energy degeneracy is also reflected in the continuum model (where the N-fold symmetry is approximated as continuous) by the rotational invariance of $E_{\rm pol}(\phi)$ (which depends only on ϕ'). The broken cylindrical to helical symmetry of the straight state is then restored by the presence of a "Goldstone mode" $\phi \to \phi + \phi_0$ consisting of a rotation of P by an arbitrary angle ϕ_0 in the material frame (cf. Figs. 2, 3). This mode comes energetically for free and leads to dramatic effects on the chain's fluctuations; for instance, for a MT clamped at one end, this symmetry implies that the MT will randomly rotate much like a rigid rotor, as shown in Fig. 4. Note however that this rotation will still be associated with a certain dissipation, as the system has to go over energy barriers between two helical states. This barrier due to the flipping of lattice states can be overcome at nonzero temperatures by the creation of double defects which diffusively propagate along the MT and eventually angularly reorient the polymorphic order parameter $\vec{P}$. These dynamic phenomena and the dissipation mechanisms will be discussed in a later section.

In summary, the zero-energy mode that we also call the "wobbling mode" is an inherent feature of a helically polymorphic filament and, as we will now see, could be the culprit causing anomalous fluctuations of clamped MTs.

Persistence length anomalies

Among several definitions of the persistence length, we consider here—for direct comparison with clamped MTs experiments (Pampaloni et al. 2006; Taute et al. 2008)—the "lateral fluctuation persistence length" defined as

$$l_{\rm p}^*(s) = (2/3)s^3/V(s), \tag{15}$$

where $V(s) = \left\langle \rho(s)^2 \right\rangle - \langle \rho(s) \rangle^2$ is the variance of $\rho^2 = x^2 + y^2$, the transverse displacement at position s, and $\langle \cdot \rangle$ is the ensemble average. As in experiments (Pampaloni et al. 2006; Taute et al. 2008), we assume a rigid clamping point at position $s = 0$, preventing the microtubule from translating and rotating at that point.

For an ideal semiflexible wormlike chain we expect that the persistence length $l_{\rm p}^* = l_{\rm B}$ is a position-independent and definition-invariant quantity equal to the bending persistence length $l_{\rm B} = B/k_{\rm B}T$. (For another more classical definition of the persistence length, coming from the tangent tangent correlation function, see also Appendix C). However for a polymorphic chain, the strict equivalence of $l_{\rm p}^*$

and l_B is not correct. To see this, we can decompose the polymorphic and elastic fluctuations $\overrightarrow{\rho}(s) = \overrightarrow{\rho}_{pol} + \overrightarrow{\rho}_{el}$. Inserting this into Eq. 15 and taking into account that, for small deflections, the two components decouple $\langle \overrightarrow{\rho}_{pol} \overrightarrow{\rho}_{el} \rangle = 0$ leads us to the following relation for the persistence length:

$$l_p^* = \left(l_{pol}^{-1} + l_B^{-1} \right)^{-1} \tag{16}$$

with the polymorphic persistence length given by $l_{pol} = (2/3)s^3/V_{pol}$ and $V_{pol} = \langle {\rho_{pol}}^2 \rangle - \langle \rho_{pol} \rangle^2$. The average $\langle \cdot \rangle$ is now performed over the phase ϕ governed by the energy Eq. 11. More precisely, the average of any arbitrary functional $A[\phi]$ of the polymorphic phase can be performed by first selecting one of the equivalent ground states characterized by $\phi(0) = \phi_0$ and then performing the average over the polymorphic angle distribution (Eq. 11) around the chosen ground state, i.e.,

$$\langle A[\phi] \rangle|_{\phi_0} = \frac{1}{Z} \int \mathrm{D}\tilde{\phi} A\left[\tilde{\phi} + \phi_0 \right] \exp\left(-\frac{l_\phi}{2} \int_0^L \mathrm{d}s \tilde{\phi}'^2 \right), \tag{17}$$

where $\tilde{\phi} = \phi - \phi_0$ (and thus $\tilde{\phi}(0) = 0$) and $Z = \int \mathrm{D}\tilde{\phi} \exp(-\frac{l_\phi}{2} \int_0^L \mathrm{d}s \tilde{\phi}'^2)$ is the partition function. In a second step, for a freely rotating polymorphic phase, we integrate over the rotational zero mode $\phi_0 : \langle A[\phi] \rangle = \frac{1}{2\pi} \int \langle A[\phi] \rangle|_{\phi_0} \mathrm{d}\phi_0$. This operation correctly takes into account the phase fluctuations over (and around) all equivalent ground states related by the transform $\phi \to \tilde{\phi} + \phi_0$. The rotational symmetry around the z axis (integration over ϕ_0) readily implies $\langle \rho_{pol}(s) \rangle = 0$ and $\langle x_{pol}^2 \rangle = \langle y_{pol}^2 \rangle$. Therefore, the polymorphic persistence length can be written as

$$l_{pol}(s) = (1/3)s^3 / \langle y_{pol}^2(s) \rangle \tag{18}$$

with

$$\langle y_{pol}^2(s) \rangle = \int_0^{2\pi} \frac{\mathrm{d}\phi_0}{2\pi} \int_0^s \int_0^s \langle \theta_{y,pol}(s_1) \theta_{y,pol}(s_2) \rangle|_{\phi_0} \mathrm{d}s_1 \mathrm{d}s_2, \tag{19}$$

whose computation (for details cf. Appendix C) leads to the following mean-square displacement:

$$\langle y_{pol}(s)^2 \rangle = \frac{2\kappa_0^2 l_\phi}{3(1 + 4l_\phi^2 q_0^2)^4} \Big\{ P_1(s) - \mathrm{e}^{-\frac{s}{2l_\phi}} P_2(s) \cos(q_0 s) - \mathrm{e}^{-\frac{s}{2l_\phi}} P_3(s) \sin(q_0 s) \Big\}, \tag{20}$$

where $P_i(s)$ are polynomial functions given in Appendix C.

A typical curve of l_p^* versus s is provided in Fig. 9. In general, it shows three different characteristic regimes, denoted I, II, and III in the figure:

(I) At short distances to the attachment point $s < s_{min} \approx \pi/q_0$ (half the polymorphic wavelength) the total persistence length can be approximately given by

$$l_p^* \approx l_B - \frac{3\kappa_0^2 l_B^2 s}{8}. \tag{21}$$

In the limit of very short distances $s \ll l_B^{-1} \kappa_0^{-2}$, the polymorphic fluctuations become negligible and are completely dominated by purely "classical" semiflexible chain fluctuations. Not surprisingly, the persistence length coincides then with the classical bending persistence length $l_p^*(0) = l_B$. Starting from l_B, polymorphic fluctuations begin to contribute, reducing l_p^*, which attains a global minimum at $s_{min} \approx \pi/q_0$.

(II) For intermediate length values $s_{min} < s < l_\phi$, the total persistence length displays a nonmonotonic, oscillatory behavior around a nearly linearly growing average

$$l_p^*(s) \approx \frac{2}{3} \frac{q_0^2}{\kappa_0^2} s + \frac{4}{3} \frac{q_0}{\kappa_0^2} \sin(q_0 s). \tag{22}$$

This result is worth deeper understanding. A moment of thought reveals that the oscillatory part with wavelength $2\pi/q_0$ is related to the helicity of the ground state. At the same time the linear growth $l_p^*(s) \propto \alpha^2 s$ can be associated with the roughly conical rotation of the clamped chain (wobbling mode) which acts as an effective "rotational hinge" at the attachment point (cf. Fig. 4). The sinusoidally modulated rotation cone which builds an approximate envelope for the chain's motion has an opening angle α which is related to the geometric features of the helix as $\alpha = 2\kappa_0 q_0^{-1}$.

(III) Finally for very large distances from the attachment point $s \gg l_\phi$ we expect to recover classical results of a semiflexible chain again. Indeed, in this asymptotic regime the effective persistence length reaches saturation with a renormalized constant value $l_p^*(\infty) = 1/\left(l_{pol}^{-1} + l_B^{-1} \right)$, where

$$l_{pol} = 2 l_\phi q_0^2 \kappa_0^{-2} + \frac{1}{2} \kappa_0^{-2} l_\phi^{-1}. \tag{23}$$

Intuitively the helix then loses its "coherent nature"—due to strong variations of ϕ' and elastic fluctuations θ_{el}—and the collective rigid rotational ("conical") motion is finally replaced by an uncorrelated segment movement. Not surprisingly, the persistence length then becomes length independent again. Curves for different values of l_ϕ are provided in Fig. 10.

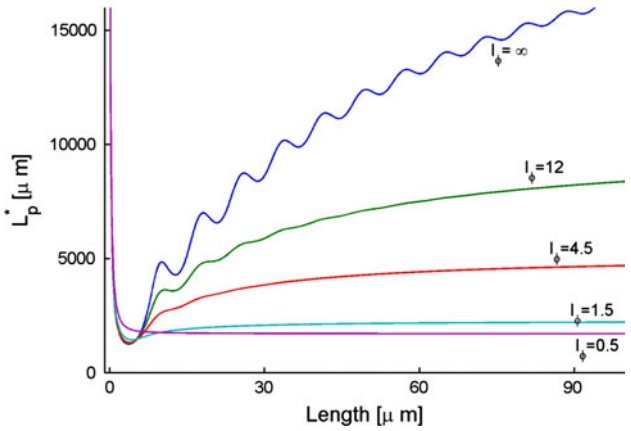

Fig. 10 Comparison of theoretical persistence lengths for different values of the polymorphic phase coherence length l_ϕ ($l_B = 25$ mm, $\kappa_0 = 0.03\ \mu m^{-1}$, and $q_0 = 0.8\ \mu m^{-1}$). For $l_\phi = \infty$, the MT is a (defect-free) coherent helix performing the "wobbling motion" (as in Figs. 4 and 8a, *left panel*). The plateau regime—where elastic fluctuations become dominant over polymorphic—is reached for very long MT only (not seen in the figure). Finite l_ϕ reduces the coherent wobbling motion, shortening region II of Fig. 9, and the plateau regime is reached earlier with decreasing l_ϕ

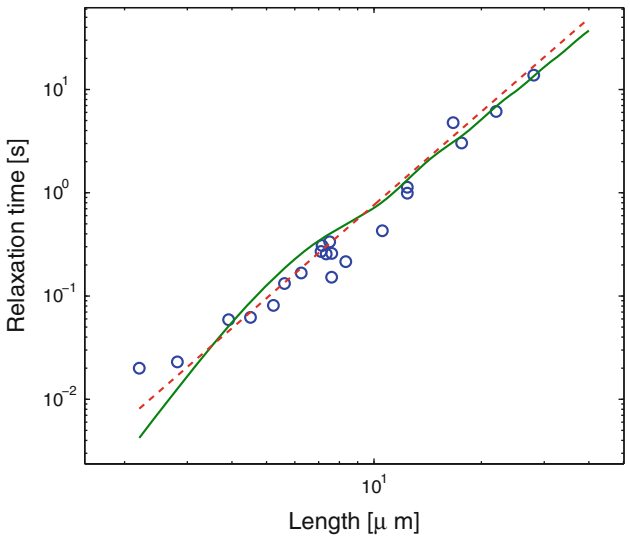

Fig. 12 The experimental microtubule relaxation times (Taute et al. 2008) and the no-adjustable-parameter theoretical prediction (full line) as obtained from static data in Fig.11 (with $l_B = 25$ mm, $\lambda = 7.5\ \mu m$, $\kappa_0^{-1} = 18\ \mu m$, and $q_0 l_\phi \gg 1$). The *dashed line* illustrates the long-length approximation (Eq. 33), displaying the characteristic cubic scaling with length

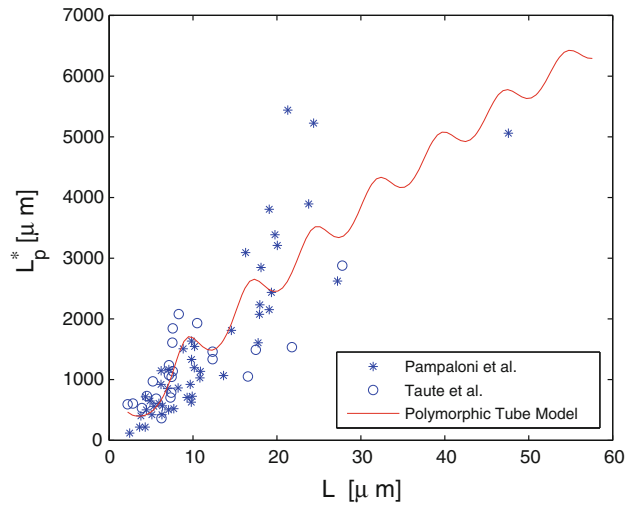

Fig. 11 Effective persistence length l_p^* as a function of position from the attachment point along the clamped MT contour: experimental data (*stars* and *circles*) (Pampaloni et al. 2006; Taute et al. 2008) and the theoretical prediction with $l_B = 25$ mm, $\lambda = 7.5\ \mu m$, $\kappa_0^{-1} = 18\ \mu m$, and $q_0 l_\phi \gg 1$

Untwisted MTs

While there are no completely twist-free MTs and every lattice will have generically a small twist, one can still formally study the interesting limiting case $q_0 = 0$. Note that the large estimated pitch of 13-PF MTs is finite and in the range of $\gtrsim 25\ \mu m$ (Wade et al. 1990; Chretien 1991, 2000; Ray et al. 1993), while often assumed to be approximately infinite. In such an ideal case the theory still applies; however, the overall behavior of $l_p^*(L)$ will substantially change and become much less consistent with the linear scaling found in experiments. While for $q_0 L > 1$ the chain to leading order moves on a linear cone (with fixed opening angle α), for $q_0 L \ll 1$ but still $L \ll l_\phi$ the "wobbling" motion occurs on a quadratic cone (a "trumpet-shaped" cone, cf. Fig. 8b). More precisely, for the exceptional case of untwisted MTs, the polymorphic part of the lateral fluctuations (Eq. 20) behaves as $\left\langle y_{pol}(s)^2 \right\rangle = 2/3\kappa_0^2 l_\phi \left(P_1 - e^{-\frac{s}{2l_\phi}} P_2 \right)$ with $P_1(s) = 24 l_\phi^3 - 3 l_\phi s^2 + s^3$, $P_2(s) = 24 l_\phi^3 + 12 l_\phi^2 s$. Therefore, for short MTs $L \ll l_\phi$, the lateral fluctuations grow with the fourth power of the length $\left\langle y_{pol}(L)^2 \right\rangle \approx \kappa_0^2 L^4/8$, whereas for long ones $L \gg l_\phi$, the deviation grows cubically, $\left\langle y_{pol}(L)^2 \right\rangle = 2/3\kappa_0^2 l_\phi L^3$. From this, the persistence length consequently has two typical regimes. For $L \ll l_\phi$ we deduce from Eqs. 16 and 18 that $l_p^*(L) \approx \left(l_B^{-1} + 3/8\kappa_0^2 L \right)^{-1}$. This expression implies that long, untwisted MTs appear increasingly softer with growing length, and the effective persistence length decays inversely $l_p^* \propto 1/L$ for $L \gg 1/(3/8\kappa_0^2 l_B)$ and reaches a limiting value $l_p^* = l_B/\left(1 + 2 l_B l_\phi \kappa_0^2\right)$ for $L \gg l_\phi$. For a MT of $L \sim 10 - 20\ \mu m$ we would expect $l_p^* \sim 10 - 20\ \mu m$, a value two orders of magnitude smaller than observed by Pampaloni et al. (2006) and Taute et al. (2008). This decreasing behavior is in contrast with observations of

$l_p^* \propto L$, leading us to the conclusion that the zero-twist MTs do not constitute a significant portion of the experimental data (Pampaloni et al. 2006; Taute et al. 2008) and that twist is necessarily required for growth of l_p^* with L.

Having developed some static consequences of the polymorphic MT we now turn to its dynamical aspects.

Polymorphic phase dynamics

To describe the MT fluctuation dynamics we consider the total dissipation functional $P_{\rm diss} = P_{\rm ext} + P_{\rm int}$, which is composed of an internal dissipation $P_{\rm int} = \frac{1}{2}\xi_{\rm int}\int \dot{\phi}^2 {\rm d}s$ (with $\dot{\phi} \equiv {\rm d}\phi/{\rm d}t$) coming from the flipping of lattice states and an external hydrodynamic dissipation $P_{\rm ext} = \frac{1}{2}\xi_\perp \int \dot{\vec{\rho}}^2 {\rm d}s$ associated with the time variation of the MT deflection $\vec{\rho}(s,t) = (x(s,t), y(s,t))$. We assume that the friction constant (per unit length) $\xi_\perp$ of the helical MT is approximately the friction constant $\xi_\perp = 4\pi\eta/(\ln(2L/R) - 1/2)$ of a long slender body of length L of (small) radius $R \ll L$ moving in a fluid with viscosity η at low Reynolds numbers. The time evolution equations of the phase variable $\phi(s, t)$ and the lateral displacement $y(s, t)$ [and $x(s, t)$] are given by the coupled Langevin equations

$$\frac{\delta E_{\rm tot}}{\delta \phi} = -\frac{\delta P_{\rm diss}}{\delta \dot{\phi}} + \Gamma_\phi \tag{24}$$

and

$$\frac{\delta E_{\rm tot}}{\delta y} = -\frac{\delta P_{\rm diss}}{\delta \dot{y}} + \Gamma_\rho \tag{25}$$

with $\Gamma_{\phi/\rho}$ the thermal noise terms. In general, the lateral displacement $y(s, t)$ has contributions from both polymorphic $y_{\rm pol}(s,t) \approx \kappa_0 \int_0^s {\rm d}s' \int_0^{s'} \sin(\phi(\tilde{s},t) + q_0 s){\rm d}\tilde{s}$ and elastic fluctuations $y_{\rm el}(s,t) \approx \int_0^s \theta_{\rm el}(s',t){\rm d}s'$ and the dynamics is highly nonlinear. In the regime $L \gg l_\phi$ where the helix loses its coherence, one expects to retrieve the dynamics of the usual semiflexible filament with $\tau \sim L^4$. However, in the opposite and physically more interesting regime $L \ll l_\phi$, a new and different dynamic behavior can be expected. As we learnt from the study of the static case the effects of polymorphism become more pronounced at shorter lengths. As we have seen in this regime, the dominant motion is the wobbling rotation of a coherent helix on a cone where elastic fluctuations become negligible compared with polymorphic ones, i.e., $y(s,t) \approx y_{\rm pol}(s,t)$. In this regime few polymorphic defects with $L \ll l_\phi$ are present and the phase can be approximated as $\phi(s,t) \approx \phi_0(t) + \delta\phi(s,t)$. Using this decomposition with $\delta\phi(s,t) \ll 1$ we can expand $P_{\rm ext}$ to leading order as

$$P_{\rm diss} \approx \frac{1}{2}L(\xi_{\rm int} + \xi_{\rm ext})\dot{\phi}_0^2 + O\left(\delta\dot{\phi}^2\right) \tag{26}$$

with an external friction constant $\xi_{\rm ext}$ given by

$$\xi_{\rm ext} = \frac{\xi_\perp \kappa_0^2}{q_0^4}\left(2(1+\cos Lq_0) - 4\frac{\sin Lq_0}{Lq_0} + \frac{q_0^2L^2}{3}\right). \tag{27}$$

The evolution of the zero mode $\phi_0(t)$ reduces from the Langevin equation (Eq. 24) to $0 = -\frac{\delta P_{\rm diss}}{\delta\dot{\phi}_0} + \Gamma_\phi$, which leads to the equation of motion

$$\frac{\rm d}{{\rm d}t}\phi_0(t) = \frac{1}{\xi_{\rm tot}}L^{-1}\int_0^L \Gamma_\phi(s,t){\rm d}s \tag{28}$$

with a friction constant $\xi_{\rm tot} = \xi_{\rm int} + \xi_{\rm ext}$. Therefore, $\phi_0(t)$ satisfies the simple Langevin equation (Eq. 28) corresponding to a simple potential–free Brownian motion with mean-square displacement given by (see Appendix D for a more detailed explanation)

$$\left\langle (\phi_0(t) - \phi_0(0))^2 \right\rangle = \frac{2k_{\rm B}T}{L\xi_{\rm tot}}t. \tag{29}$$

In this limit (wobbling mode dominant), we have a roughly rigid helix moving randomly along a cone and all the physics is contained in the effective friction coefficient $\xi_{\rm tot}(\xi_{\rm int}, \kappa_0, q_0, L)$ and its dependence on the internal dissipation $\xi_{\rm int}$, the helix parameters κ_0, q_0, and the length L.

For later comparison with experiments we compute the longest relaxation time τ given by the autocorrelation function $\langle y_{\rm pol}(s,0)y_{\rm pol}(s,t)\rangle \propto {\rm e}^{-t/\tau}$. Using Eq. 29, a short computation (Appendix D) leads to

$$\left\langle y_{\rm pol}(L,0)y_{\rm pol}(L,t)\right\rangle = \left\langle y_{\rm pol}^2(L)\right\rangle {\rm e}^{-t/\tau(L)} \tag{30}$$

with $\left\langle y_{\rm pol}^2(L)\right\rangle = \frac{\kappa_0^2}{q_0^2}\left(\frac{L^2}{2} + \frac{1-\cos(q_0L)}{q_0^2} - \frac{L\sin(q_0L)}{q_0}\right)$ as the static mean-square displacement (Eq. 20) in the limit $L \ll l_\phi$ and with $\tau(L) = L\xi_{\rm tot}/k_{\rm B}T$ as the longest relaxation time, proportional to the total friction constant $\xi_{\rm tot}$. For very short lengths $L \ll l_{\rm c} = (3\xi_{\rm int}\xi_\perp^{-1})^{1/2}q_0\kappa_0^{-1}$ when the hydrodynamic dissipation is entirely dominated by internal dissipation, we have a linear scaling

$$\tau(L) \approx L\xi_{\rm int}/k_{\rm B}T. \tag{31}$$

For larger $L > l_{\rm c}$, the wobbling movement through the fluid is the dominant source of dissipation and

$$\tau(L) \approx L\xi_{\rm ext}(L)/k_{\rm B}T \tag{32}$$

with $\xi_{\rm ext}(L)$ given by Eq. 27. Note that the L dependence of $\xi_{\rm ext}$ relies also on the L dependence of $\xi_\perp(L)$, which for simplicity has been modeled as the friction of an ideal slender tube moving in a liquid. A more precise (but difficult) determination of $\xi_\perp$ could slightly change its

variation with L, although not the general trends of $\xi_{\text{ext}}(L)$. In particular, if we assume that $\xi_\perp$ is L independent and that $Lq_0 \gg 1$, we have in this regime the scaling

$$\tau(L) \approx \frac{\xi_\perp}{3k_BT}(\kappa_0/q_0)^2L^3. \quad (33)$$

So in summary for τ we expect a crossover from a linear, internal-dissipation-dominated L dependence at short lengths to a cubic length dependence given by hydrodynamic friction alone.

Comparison with clamped MT experiments

Comparison with experiments (Pampaloni et al. 2006; Taute et al. 2008) which measured lateral fluctuations of clamped MTs reveals several interesting characteristics that are in agreement with predictions (cf. Fig. 11). First, the predicted mean linear growth of $l_p^*(L)$ agrees with experiments, as a single exponent fit $l_p^* \sim L^\delta$ of the data yields $\delta = 1.05$. Besides the linear growth, the experimental data reveal a large spread of l_p^* data points which seems to grow approximately in proportion to the length. This linearly growing experimental spread is likely linked to the intrinsic spread of q_0 values of different MT lattice populations (Wade et al. 1990; Chretien 1991, 2000; Ray et al. 1993). MTs with different number of protofilaments will display different lattice twists ranging from $q_0 \approx 2\pi/3$ μm (for 12-PF MTs) to $q_0 \lesssim 2\pi/25$ μm (for 13-PF MTs). Keeping in mind the scaling $l_p^*(s) \propto q_0^2 s$ (cf. Eq. 22), we would expect more than an order of magnitude variation of measured l_p^* values while the slope $l_p^*(s)/s$ should display a constant spread.

Second, the data of Taute et al. (2008) (Fig. 11, circles) indicate a nonmonotonic dependence with systematic trends over several consecutive data points. This seems to be phenomenologically well captured by the oscillatory behavior of $l_p^*(L)$ in Eq. 22. On the other hand, the data of Pampaloni et al. (2006) are definitely much more spread and do not allow such a clear conclusion. Therefore, the nonmonotonicity of $l_p^*(L)$ is at present experimentally difficult to confirm from the two existing experimental datasets taken together, although it is consistent with the data within the error bars. As mentioned, the presence of different lattice populations (even within single MTs) could give rise to a large spread of experimental data points and an effective "washing out" of the nonmonotonic behavior for different lattices within the same statistics.

Remarkably, the experimental data reveal that the large-length plateau $s \gg l_\phi$ where l_p^* would become length independent is not reached even for the longest MTs ($\sim$50 μm). This is in phenomenological agreement with the theory, as based on the long coherent helices observed by Venier et al (1994) it would imply a very long l_ϕ. The absence of the plateau in Pampaloni and Taute's data allows a lower estimate of the coherence length: $l_\phi > 55$ μm, which in turn would imply a large coupling constant $J > 4k_BT$. The best comparison between theory and experiments (cf. Fig. 11) gives $l_B = 25$ mm, corresponding to a rather high Young's modulus $Y \approx 9$ GPa higher than typically reported before (Gittes et al. 1993; Venier et al. 1994; Mickey and Howard 1995; Felgner et al. 1996; Kikumoto et al. 2006; Kurachi et al. 1995; Takasone et al. 2002; Brangwynne et al. 2007; Janson 2004). However, the present value is well within the range for proteins and protein tubes, with Y up to 19 GPa being reported in literature (Kol et al. 2005). The higher value of the bare Young's modulus extracted form the present theory should also not be a surprise, as in previous models all MT conformational fluctuations were interpreted as originating from bending deformations alone. In our model, both elastic and polymorphic fluctuations contribute, with the latter being much softer and giving therefore dominant contribution.

The best-fitting helix wavelength $\lambda \approx 7.5$ μm is close to the expected 6 μm corresponding to the twist (Wade et al. 1990; Chretien 1991, 2000; Ray et al. 1993) of the 14-PF MT population. This is in agreement with the fact that, in contrast to the in vivo situation, the large-pitch ($\lambda \approx 25$ μm) 13-PF MTs are likely underrepresented in the data (Pampaloni et al. 2006; Taute et al. 2008). Indeed, in vitro studies of taxol-copolymerized MTs display a MT population consisting of a majority of 14 PFs (61%) while 13 PFs (32%) are less represented (Wade et al. 1990; Chretien 1991, 2000; Ray et al. 1993). The in vitro conditions therefore strongly shift the PF population away from the preferred low-twist 13-PF MT towards the highly twisted 14-PF MT.

The estimated l_B is larger than in previous studies ($l_B \approx$ 1–6 mm), where however polymorphic fluctuations were neglected. This result leads us to the conclusion that, if polymorphism is partially suppressed, one would measure much larger effective l_p, as is in fact observed; for example, in studies where 2D slab geometry is used (MTs between two close glass slides), effective suppression of the three-dimensional polymorphic helices or reduction of their mobility is expected. A typical observation in such cases is an extensive "intrinsic curvature" (of previously unknown origin). Within our theory one could interpret this curvature as pinned/quenched polymorphic helices prevented from fluctuating freely by the confinement. These effects could in general explain the dramatic variations of measured l_p values based on the presence/absence of polymorphic "softening" in different experimental setups and geometries.

Now, let us consider the clamped MT dynamics as investigated by Taute et al. (2008). Careful analysis of Taute et al.'s data reveals a peculiar scaling of the longest relaxation time with the length. Indeed, an independent single exponent fit of Taute et al.'s data (2008) gives $\tau \propto L^{\alpha}$ with $\alpha = 2.9$ in the experimental range considered ($2.2\ \mu\text{m} < L < 28\ \mu\text{m}$). This peculiar scaling can be understood as originating from hydrodynamic relaxation of a "wobbling" polymorphic chain. Using only the previously best-fitting parameters of the static data (Fig. 11) $(\kappa_0/q_0)^2 \approx 4.8 \times 10^{-3}$ and $\eta = 10^{-3}$ Pa·s (viscosity of water), we find a remarkable correspondence between the theoretical prediction (Eq. 32), i.e., $\tau_{\text{th}}(L) \approx L\xi_{\text{ext}}(L)/k_{\text{B}}T$ and the data of Taute et al. (2008), as shown in Fig. 12. This zero-parameter prediction matches well the data for larger lengths. For scaling comparison, it is interesting to compare the data with the approximate theoretical relaxation time (Eq. 33), i.e., $\tau(L) \approx \frac{\xi_{\perp}}{3k_{\text{B}}T}(\kappa_0/q_0)^2 L^3$ (expression strictly valid for $L \gg 0.8\ \mu\text{m}$), which has a scaling law in agreement with the single exponent fit of the data. Considering that $\xi_{\perp} \approx 1.6\eta - 2.3\eta$ is roughly length independent in the experimental L range, one can assume $\xi_{\perp} \approx 2\eta$ to obtain the prefactor as $\tau_{\text{th}}/L^3 = 7.9 \times 10^{14}$ s/m^3. Keeping in mind the simplicity of the interpretation (and the lack of free parameters therein), this compares very favorably with the best fit to the experimental data slope $\tau_{\text{fit}}/L^3 = 6.\ 25 \times 10^{14}$ s/m^3 (cf. Fig. 12). Note that the approximate value of τ_{th} seems to correspond slightly better to the data, but this is likely of no physical significance at this level of approximation. Indeed, the neglected elastic modes other than the wobbling as well as the approximation of the hydrodynamic friction should change the details of the L dependence of ξ_{ext} and thus of τ_{th} (but not the general trends). Without more precise computation of the dynamics we can be satisfied with the rather astonishing agreement between theory and experiment for long MTs. This leads us again to the conclusion that, in these experiments, long MTs behave as almost rigid helical polymorphic rotors whose motion is dominated by the zero-energy "wobbling" mode and its hydrodynamic dissipation.[1]

For very short MTs we should expect deviation from this simple interpretation. In this regime the linearly scaling internal dissipation, coming from the migration of polymorphic defects, should start to dominate over pure hydrodynamic friction, and for sufficiently short MT lengths $L \to 0$ we could measure ξ_{int} from the limit value of τ_{th}/L. It appears that, for the presently available data with $L > 2\ \mu\text{m}$ (Taute et al. 2008), this plateau regime is not yet fully developed, enabling us to provide only an upper numerical estimate for the inner dissipation $\xi_{\text{int}} \lesssim 4 \times 10^{-17}$ Ns.

[1] In Appendix E we discuss possible effects induced by surface attachment that could to some extent interfere with the ideal free "wobbling" motion in experiments.

Very short MTs

Comparison with experiments for even shorter chains ($L < \pi/q_0$) is more difficult due to the lack of data in clamped MT experiments ($L > 2\ \mu\text{m}$). We can nevertheless try a comparison with the results by the Dekker group for the kinesin motor gliding assay of short MTs (Vanden Heuvel et al. 2007, 2008). Besides some similarities with the clamped fluctuating MTs, there are a number of differences between the modeled situation of free 3D MTs and the 2D gliding assay. In particular, the 2D geometry will strongly perturb the preferentially three-dimensional helical ground state. The active contribution of strong motor forces to the trajectory of short MTs is an additional potential perturbation. Effects of MT buckling and axial MT rotation by kinesins likely become important. This said and ignoring the differences, we can still compare (in order of magnitude) our and the Dekker group's results (Vanden Heuvel et al. 2007, 2008). For micron-sized MTs we obtain $l_{\text{p}} \approx 0.8\ \mu\text{m}$, in approximate agreement with the $\sim 0.2\ \mu\text{m}$ value obtained by Vanden Heuvel et al. (2007). One should mention that the two cited studies (Vanden Heuvel et al. 2007, 2008) give strongly different results depending on whether free gliding or gliding assay with additional electric field is considered. This difference results from the larger deformations induced by the electric field. Therefore, the comparison of our theory with the passive gliding assay appears more appropriate and gives closer agreement.

Summary

We have suggested a new model that connects some of the most persistent and confusing experimental findings concerning microtubules. Starting from a rather broad spectrum of (apparently) disconnected observations, we progressively built the case for a new hypothesis: the existence of internal switching of the GDP–tubulin dimer within the microtubule lattice. Why do microtubules become helically wavy? Why do they switch to permanently bent circular states? Why do they fluctuate anomalously when clamped? These three dangling questions became the central pillars for the present model. Surprisingly, the simple assumption of a bistable GDP–tubulin seems to explain these otherwise disparate phenomena in a unified manner. As we know from recent experiments, the bistability hypothesis of taxol-stabilized protofilaments is indeed empirical fact (Elie-Caille et al. 2007). We have shown here that the incorporation of such a bistable tubulin

into a closed elastic lattice changes its free behavior, introducing strong conformational competition among the tubulin dimers. Tubulin units on opposite sides of the tube now start to compete for which is going to switch to the curved state. The lattice-induced frustration does not allow all the tubulin dimers to minimize their energy individually and to switch to their preferred states at the same time. The symmetry breaking induced by this frustration mechanism leads to a global microtubule lattice curving. Remarkably, the curving direction is chosen randomly, and this has profound consequences. The microtubule can chose between many energetic ground states (as many states as protofilaments in the lattice). When we graft one end of the microtubule onto a substrate while still allowing it to chose its bending direction freely, the strange energy degeneracy generates a very unusual thermal motion. In this case the microtubule's motion follows, roughly speaking, a cone and it rotates or "wobbles" at no energy cost around its attachment tangent. This mode of motion, which is not to be confused with material frame rotation (which is strictly prohibited by grafting), is probably among the most striking outcomes of the two-state GDP–tubulin model. It is exactly this behavior that allows consistent explanation of the measurements of unusual lateral fluctuations of grafted microtubules (Pampaloni et al. 2006; Taute et al. 2008).

Perspectives

We focus herein on modeling taxol-stabilized microtubules, and the question naturally arises if the proposed model affects "real" in vivo microtubules. On the one hand the "weakly curved" state that is involved in the soft polymorphic dynamics as described here seems to be (so far) a specific signature of taxol-stabilized GDP–tubulin state. On the other hand, we have argued that the naturally occurring "high-curvature" GDP–tubulin state could coexist with the straight state in the lattice under in vivo conditions where MTs are stabilized with MAPs. The involvement of this high-curvature state switching seems to manifest itself in motor-driven straight to wavy transitions of MTs in many living cell systems (Bicek et al. 2009; Brangwynne et al. 2006, 2007; Keating et al. 1997; Kaech et al. 1996; Samsonov et al. 2004). A particularly impressive instance of such a polymorphic switching event in vivo could be found in the process of axonal retraction, where the whole MT cytoskeleton of the axon undergoes a straight to helical transition and in turn retracts towards the soma (Fridoon et al. 2000). To understand these dramatic transitions in vivo, the present theory has to be advanced and modified in two ways. First, the effect of large active motor forces (rather than thermal ones) has to be taken into account. In particular, one expects that, under strong buckling forces, even thermodynamically unfavorable states can become activated and constitute the ground state upon large loads.

Second, in virtually all in vivo experiments, MTs are essentially confined in 2D as the containing cells adsorb to the glass substrate and assume a vary flat "fried-egg" configuration. Consequently, the measured properties will not necessarily reflect the three-dimensional properties of the molecule. This is particularly important for a MT transformed to a polymorphic helix state where the confinement naturally entails a strong deformation (of the initially three-dimensional ground state). Under confinement the helical bending and torsional modes become strongly coupled and bring about new physical effects. In particular, a torsionally very soft helix will have a tendency to unwind and form in extreme cases circular arcs, reminiscent of the rings observed in gliding assay experiments (Amos 1991).

Finally, the local action of molecular motors could trigger a switching to the highly curved state. While for classical motors such as kinesin 1 direct evidence for such a mode of action is still lacking, its relative kinesin 13 (Elie-Caille et al. 2007; Desai et al. 1999) has a well-documented ability to actively trigger radial bending of protofilaments. Other molecules such as katanin (Hartman et al. 1998; Davis et al. 2002) have also been suggested to perturb the lattice and trigger longer-range transitions (Mohrbach 2007). This opens the intriguing question of whether classical motors (kinesin 1 and dynein) could trigger cooperative state transitions and even transmit conformational signals along the tube. Considering the present model for stabilized MTs (where high cooperativity is inherent to the data interpretation), this idea might not be far fetched. In fact, some evidence towards long-range cooperativity of kinesin binding along the MT was presented by Muto et al. (2005), although these results still await robust reproduction.

This brings us to the question of what experiments should be performed in order to nail down the polymorphic mechanism or any other mechanism for MT dynamics. With microtubules being such delicate, subtle, and possibly long-range-correlated objects (as suggested here), a general rule of thumb for experiments should be: Treat them more gently (do not confine) and observe more carefully (look for correlated motion). A simple yet important experiment would be a systematic direct observation of one-side grafted but otherwise *completely unconfined* MTs fluorescently labeled *along their full contour length*. As mentioned, the presence of a quasi-2D confinement in thin chambers as used in most MT experiments so far would perturb the native helical MT state and should therefore be explicitly avoided. The freely suspended gold-EM nanogrid attachment geometry as used by Pampaloni et al.

seems particularly suited for this task. Going beyond Pampaloni et al., who labeled and traced the MT end only (via a bead), the microtubules should be visualized along the full contour in this geometry. Tracing several or all points along the contour should reveal the predicted sinusoidal–helical nature of MT states. The present model predicts a peculiar cooperatively rearranging helix state with characteristic telltale curvature correlations between different lattice positions, which are entirely absent for usual semiflexible filaments. Directly observing collective motions such as the suggested "wobbling" mode while prohibiting trivial spatial rotations that could mask the effects (by MT grafting) would constitute "smoking-gun" evidence for a polymorphism-related mechanism.

In conclusion, we have proposed a novel model for internal MT lattice dynamics. We have shown that it accounts for the otherwise mysterious MT helicity (Venier et al. 1994) and the anomalous length-dependent lateral fluctuation static (Pampaloni et al. 2006; Taute et al. 2008) and dynamic scaling (Taute et al. 2008). The latter two phenomena appear as mere consequences of the peculiar "wobbling motion" of the polymorphic, cooperatively switching MT lattice. Although most of the observations discussed here were made in vitro on taxol-stabilized MTs, we provide arguments in favor of the existence of polymorphic MT states in vivo. We speculate that the implied conformational bistability of tubulin and the allosteric interaction are more than just nature's way of modulating the elastic properties of its most important cytoskeletal mechano-element. It could also be a missing piece in the puzzle of polymerization "catastrophes." Even more intriguingly, the predicted structural cooperativity could allow for long-range conformational signaling along single MTs and turn the latter into an efficient "confotronic" wire transmitting regulatory signals across the cell.

Acknowledgments We acknowledge fruitful discussions with Francesco Pampaloni, Denis Chrétien, Thomas Surrey, Francois Nédélec, Jean-Francois Joanny, Sergey Obukhov, Linda Amos, and André E.X. Brown and thank Falko Ziebert for discussion and useful comments on the manuscript.

Appendix

A. Polymorphic phase coherence length

In this section, we derive the formula $l_\phi = \frac{N^2 b}{8\pi^2}\left(2 + e^{2J/k_B T}\right)$ for the polymorphic phase coherence length. To this end we want to calculate the distribution of double junctions that leads to angular orientation change $\Delta\Phi$ on a scale l much larger than the tubulin dimer b, yet still much smaller than the total length, i.e., $b \ll l \ll L$. In this domain, at each cross-section we have three possibilities:

1. State $j = 0$ with no double defect. The rotation angle $\Delta\Phi$ is attached to the internal lattice rotation, $\frac{\Delta\Phi}{b} - q_0 = 0$.
2. State $j = -1$ for a left-handed double defect; $\Delta\Phi$ deviates from the internal twist: $\frac{\Delta\Phi}{b} - q_0 = -\frac{1}{b}\frac{2\pi}{N}$.
3. State $j = +1$ for a right-handed double defect with $\frac{\Delta\Phi}{b} - q_0 = +\frac{1}{b}\frac{2\pi}{N}$.

On a length l we are throwing a three-sided dice l/b times and the total rotation of $\Delta\Phi$ away from the optimal twist is $\Delta\Phi - q_0 l = \frac{2\pi}{N}\sum_{n=1}^{l/b} j_n$. The variation of the polymorphic phase with respect to the internal twist is then

$$\Delta\phi = \frac{\Delta\Phi}{l} - q_0 = \frac{1}{l}\frac{2\pi}{N}\sum_{n=1}^{l/b} j_n.$$

For $l/a \gg 1$ the law of large numbers implies that the random variable $\Delta\phi = \frac{1}{l}\frac{2\pi}{N}\sum_{n=1}^{l/b} j_n$ becomes Gaussian distributed

$$p(\Delta\phi) \propto e^{-\frac{\Delta\phi^2}{2\langle\Delta\phi^2\rangle}}$$

with mean $\langle\Delta\phi\rangle = 0$ and $\langle\Delta\phi^2\rangle = \left(\frac{1}{l}\frac{2\pi}{N}\right)^2\left(\frac{l}{b}\right)\langle j^2\rangle$ (as $\langle j_n j_m\rangle = \delta_{nm}\langle j^2\rangle$). The average $\langle j^2\rangle$ is given from the Boltzmann factors of the three different states $p_0 = \frac{1}{1+2e^{-2\beta J}}$ and $p_{\pm 1} = \frac{e^{-2\beta J}}{1+2e^{-2\beta J}}$, so that $\langle j^2\rangle = \frac{2e^{-2\beta J}}{1+2e^{-2\beta J}}$. We can now interpret the quantity $1/\left(2\langle\Delta\phi^2\rangle\right)$ as coming from an effective elastic energy over the interval l by writing $\frac{\Delta\phi^2}{2\langle\Delta\phi^2\rangle} = \frac{1}{2}\beta C_\phi l(\Delta\phi)^2$, which allows us to identify the effective stiffness

$$C_\phi = kT\frac{N^2}{8\pi^2}\left(2 + e^{2J\beta}\right)b.$$

Note that this expression is valid for large enough J suppressing higher-order defects, i.e., in the limit when multiple double defects sitting on a single lattice site (i.e., $|j| > 1$) can be ignored.

B. The variation of the polymorphic modulus

In this appendix we compute the energy variation due to a deviation of the polymorphic modulus $|P|$ away from its optimal value $|P^*|$ minimizing the energy, i.e., the change of the number of switched PFs. We start with the energy density of a MT cross-section

$$e = \frac{B}{2}\left(\left(\kappa - \kappa_{\mathrm{pol}}(p)\right)^2 + \kappa_1^2\left(\gamma\frac{\pi}{N}p - \sin^2\left(\frac{\pi}{N}p\right)\right)\right), \qquad (34)$$

whose minimum is reached for $p^* = \frac{N}{2} - \frac{N}{2\pi}\arcsin\gamma$. Assuming a continuous number of PFs, the energy of a state with $p = p^* + \Delta p$ switched PFs reads to quadratic order

$$e(p^* + \Delta p) \approx e(p^*) - \frac{\pi^2 B}{N^2}\kappa_1^2 \cos\left(\frac{2\pi}{N}p^*\right)\Delta p^2$$
$$= e(p^*) + \frac{\pi^2 B}{N^2}\kappa_1^2\sqrt{1-\gamma^2}\Delta p^2,$$

where we used $\cos(\pi - \arcsin\gamma) = -\sqrt{1-\gamma^2}$. Therefore, the energy variation of a segment of length l reads

$$\Delta E \approx \frac{\pi^2 B}{N^2}\kappa_1^2\sqrt{1-\gamma^2}\int_0^l \mathrm{d}s(p(s) - p^*(s))^2.$$

Now using $|P(s)| = \left|\sin\left(\frac{\pi}{N}p\right)\right| / \sin(\pi/N)$ we can write the energy variation to the same (quadratic) order as

$$\Delta E \approx B\kappa_1^2 \sin^2(\pi/N)\sqrt{1-\gamma^2}\int_0^l \mathrm{d}s((|P(s)| - |P^*|))^2.$$

Therefore, any deviation of P from its optimum state P^* is associated with an energy cost proportional to the length l of the region in the unfavorable state.

C. Persistence length(s)

A definition of the persistence length, often used in single-molecule experiments, is expressed in terms of the lateral deviation $\overrightarrow{\rho} = (x(s), y(s))$ of a MT clamped at $s = 0$ from its attachment axis as $l_\mathrm{p}^*(s) = (2/3)s^3 / \left\langle \left(\overrightarrow{\rho}(s) - \left\langle \overrightarrow{\rho}(s)\right\rangle\right)^2\right\rangle$, where $\langle\cdot\rangle$ is the statistical average. The equivalence of the x and y directions implies that $l_\mathrm{p}^*(s) = 1/3s^3 / \left\langle (y(s) - \langle y(s)\rangle)^2\right\rangle$. The second often used alternative but more standard definition of the persistence length—the tangent persistence length—is related to the angular correlation $l_\mathrm{p}(s - s') = |s - s'|/V(s - s')$ with variance $V = \left\langle \left(\theta_y(s) - \theta_y(s')\right)^2\right\rangle$ (by symmetry we have the same expression with θ_x). Whereas for an ideal WLC $l_\mathrm{p}^* = l_\mathrm{p} = l_\mathrm{B}$ is position and definition independent, this is not the case for a polymorphic chain (see Fig. 13). For small angular deformations, the decoupling of the chain's fluctuations into polymorphic and purely elastic contributions allows one to decompose the persistence length as $l_\mathrm{p}^{-1} = l_\mathrm{pol}^{-1} + l_\mathrm{B}^{-1}$, this result being valid for both definitions of the persistence length.

We first focus on the first definition, for the clamped persistence length. In this case the polymorphic persistence length $l_\mathrm{pol}^*(s)$ is given by

$$l_\mathrm{pol}^*(s) = 1/3s^3 / \left\langle \left(y_\mathrm{pol}(s) - \left\langle y_\mathrm{pol}(s)\right\rangle\right)^2\right\rangle, \tag{35}$$

where $y_\mathrm{pol}(s)$ is the lateral polymorphic displacement in the y direction. Integrating over the rotational zero mode readily implies $\left\langle y_\mathrm{pol}(s)\right\rangle = 0$ (see Eq. 18). From Eq. 19 one can write

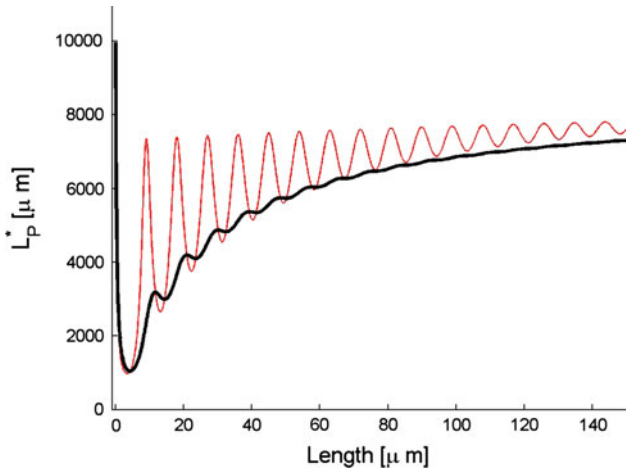

Fig. 13 Different definitions of the persistence length can deviate from each other for a polymorphic chain: the "clamped persistence length" l_p^* (*thick line*) and the "tangent persistence length" l_p (*thin line*) (for $l_\mathrm{B} = 10$ mm, $l_\phi = 50$ μm, $\kappa_0 = 0.03$ μm^{-1}, and $q_0 = 0.7$ μm^{-1})

$$\left\langle y_\mathrm{pol}^2(s)\right\rangle = \int_0^s\int_0^s G(s_1, s_2)\mathrm{d}s_1\mathrm{d}s_2$$

with the angular correlation function $G(s_1, s_2) = \left\langle\theta_{y,\mathrm{pol}}(s_1)\theta_{y,\mathrm{pol}}(s_2)\right\rangle$ given by the integration over the zero mode

$$G(s_1, s_2) = \int_0^{2\pi}\frac{\mathrm{d}\phi_0}{2\pi}G_0(s_1, s_2, \phi_0) \tag{36}$$

of the angular correlation function at fixed value of ϕ_0, i.e., $G_0(s_1, s_2, \phi_0) = \left\langle\theta_{y,\mathrm{pol}}(s_1)\theta_{y,\mathrm{pol}}(s_2)\right\rangle|_{\phi_0}$. This last expression, from the relation $\theta_{y,\mathrm{pol}}(s) = \kappa_0\int_0^s \sin\left(\widetilde{\phi}(s') + q_0 s' + \phi_0\right)\mathrm{d}s'$ (cf. Eq. 17), is explicitly given by

$$G_0(s_1, s_2, \phi_0) = \kappa_0^2\int_0^{s_1}\int_0^{s_2}\left\langle\sin\left(\widetilde{\phi}(s) + q_0 s + \phi_0\right)\right.$$
$$\left.\sin\left(\widetilde{\phi}(s') + q_0 s' + \phi_0\right)\right\rangle|_{\phi_0}\mathrm{d}s\mathrm{d}s'. \tag{37}$$

After integration over ϕ_0 and using the known result $\left\langle\cos\left(\widetilde{\phi}(s_1) - \widetilde{\phi}(s_2)\right)\right\rangle = \mathrm{e}^{-|s_1 - s_2|/2l_\phi}$ which results from the WLC-type probability distribution of the field $\widetilde{\phi}$, i.e., $P[\widetilde{\phi}] \sim \exp(-\frac{l_\phi}{2}\int_0^L \mathrm{d}s\widetilde{\phi}'^2)$, one obtains the rotational invariant correlation function in the form

$$G(s_1, s_2) = \frac{\kappa_0^2}{2}\int_0^{s_1}\int_0^{s_2}\mathrm{e}^{-\frac{|s - s'|}{2l_\phi}}\cos(q_0(s - s'))\mathrm{d}s\mathrm{d}s'. \tag{38}$$

Computation of the integrals in Eq. 38 gives finally the following expression for the polymorphic contribution to the transverse displacement:

$$\left\langle y_{\rm pol}(s)^2 \right\rangle = \frac{2\kappa_0^2 l_\phi}{3(1+4l_\phi^2 q_0^2)^4}\left\{P_1 - {\rm e}^{-\frac{s}{2l_\phi}}P_2\cos(q_0 s) + {\rm e}^{-\frac{s}{2l_\phi}}P_3\sin(q_0 s)\right\} \tag{39}$$

with $P_1(s)= 24l_\phi^3(1-6x+x^2)-3l_\phi(1+x-x^2-x^3)s^2 + (1+3x+3x^2+x^3)s^3$, $P_2(s)= 24l_\phi^3(1-6x+x^2) + 12l_\phi^2(1-2x-3x^2)s$, and $P_3(s) = 192l_\phi^4 q_0(1-x) + 24l_\phi^3 q_0(3+2x-x^2)s$, where we have introduced the notation $x = 4l_\phi^2 q_0^2$.

From Eq. 39, we get the polymorphic persistence length $l^*_{\rm pol}(s)$ defined in Eq. 35, and in turn the global persistence length $l^*_{\rm p}(s)$ depicted in Fig. 13. Its physical interpretation is discussed in the main text.

We now consider the second definition of the persistence length $l_{\rm p}(s-s') = |s-s'|/V(s-s')$. From Eq. 38, the angular variance $V_{\rm pol}$ can easily be evaluated as

$$V_{\rm pol}(s) = \frac{2\kappa_0^2 l_\phi}{1+4l_\phi^2 q_0^2}\left(s - \frac{2l_\phi\left(1-4q_0^2 l_\phi^2\right)}{1+4l_\phi^2 q_0^2}\right) + \frac{4\kappa_0^2 l_\phi^2 {\rm e}^{-\frac{s}{2l_\phi}}}{\left(1+4l_\phi^2 q_0^2\right)^2}\left(\left(1-4q_0^2 l_\phi^2\right)\cos(q_0 s) - 4q_0 l_\phi \sin(q_0 s)\right) \tag{40}$$

The resulting persistence length $l_{\rm p}$ (depicted in Fig. 13) shows a rich behavior similar to the persistence length $l^*_{\rm p}(s)$ but displays a functional form distinct from the latter. However, as expected, both curves reach the same asymptotic value at very short and very long MT lengths.

D. Zero-mode dynamics

The evolution of the zero mode $\phi_0(t)$ is given by Eq. 28 as

$$\frac{\rm d}{{\rm d}t}\phi_0(t) = \frac{1}{\xi_{\rm tot}}L^{-1}\int_0^L \Gamma_\phi(s,t){\rm d}s \tag{41}$$

with a friction constant $\xi_{\rm tot} = \xi_{\rm int} + \xi_{\rm ext}$, where $\xi_{\rm ext}$ is given by Eq. 27. The correlation function of the thermal white noise $\Gamma_\phi(s,t)$ is $\left\langle \Gamma_\phi(s,t)\Gamma_\phi(s',t')\right\rangle = D\delta(s-s')\delta(t-t')$ with a coefficient D that can be determined in the following manner. Notice first that ϕ_0 performs free Brownian motion and that its quadratic fluctuations necessarily satisfy the relation $\left\langle (\phi_0(t)-\phi_0(0))^2\right\rangle = \frac{2k_{\rm B}T}{L\xi_{\rm tot}}t$. On the other hand, integrating Eq. 41 yields

$$\phi_0(t) - \phi_0(0) = \xi_{\rm tot}^{-1}\int_0^t\left(\frac{1}{L}\int_0^L \Gamma(s,t'){\rm d}s\right){\rm d}t', \tag{42}$$

and exploiting the white noise type auto-correlation of Γ one obtains $\left\langle (\phi_0(t)-\phi_0(0))^2\right\rangle = \frac{D}{\xi_{\rm tot}^2 L}t$, from which we readily deduce $D = 2\xi_{\rm tot}k_{\rm B}T$, as expected from the fluctuation–dissipation theorem.

The relaxation time is generally given from the time correlation function $<y_{\rm pol}(s,0)y_{\rm pol}(s,t)>$ with the lateral position $y_{\rm pol}(s,t) = \frac{\kappa_0}{q_0^2}(sq_0\cos(\phi_0(t)+\alpha) + \sin(\phi_0(t)+\alpha) - \sin(q_0 s+\phi_0(t)+\alpha))$ obtained from Eq. 14 with $l_\phi \gg s$. The average must first take into account all statistically equivalent values of angular orientations $\alpha \in [0,2\pi]$, such that $\left\langle y_{\rm pol}(s,0)y_{\rm pol}(s,t)\right\rangle = \int_0^{2\pi}\left\langle y_{\rm pol}(s,0)y_{\rm pol}(s,t)\right\rangle_\alpha \frac{{\rm d}\alpha}{2\pi}$, and we obtain

$$\left\langle y_{\rm pol}(s,0)y_{\rm pol}(s,t)\right\rangle = \left\langle y_{\rm pol}^2(s)\right\rangle\left\langle\cos(\phi_0(t)-\phi_0(0))\right\rangle \tag{43}$$

with $<y_{\rm pol}^2(s)> = \frac{\kappa_0^2}{q_0^2}\left(\frac{s^2}{2} + \frac{1-\cos(q_0 s)}{q_0^2} - \frac{s\sin(q_0 s)}{q_0}\right)$, corresponding to the static result (Eq. 39) in the limit $s/l_\phi \ll 1$. With 42 defining a simple Gaussian random walk process, one straightforwardly obtains

$$\left\langle\cos(\phi_0(t)-\phi_0(0))\right\rangle = {\rm e}^{-t/\tau} \tag{44}$$

with the relaxation time given by

$$\tau = L\frac{\xi_{\rm tot}}{k_{\rm B}T}. \tag{45}$$

E. Comment on MT surface attachment and the robustness of "wobbling"

Throughout this work we have assumed that the free rearrangement of the polymorphic lattice states is not significantly hindered by the covalent surface attachment of the MT, as e.g. performed by Pampaloni et al. (2006) and Taute et al. (2008). This assumption is integral to the "wobbling" motion and in turn to understanding the static and dynamic data scaling. It therefore deserves closer consideration.

In the experiments by Pampaloni et al. (2006) and Taute et al. (2008), the adsorbed MT part is attached to a gold (electron microscopy grid) surface via thiol groups. It is likely that ≈1–2 protofilaments will establish localized chemical contacts with the gold microgrid. While substantial perturbation of the dimer such as denaturation appears unlikely, it is unclear to what extent this procedure will perturb the inner (polymorphic) dynamics of the entire tubulin dimer units. In principle, one can anticipate two

plausible scenarios that would interfere to a varying degree with the free "wobbling" motion:

S1. Due to high cooperativity (large coupling J) the polymorphic state transition can propagate within a certain penetration depth into the adsorbed (straight-planar) MT section.

S2. The cooperativity is too weak to compete with the constraints imposed by the surface (including chemical perturbations), and the polymorphic transition does not propagate into the straight adsorbed MT section.

In both cases we have a nonvanishing deflection angle between a forced (adsorbed) planar section and the free helical section direction, effectively causing the characteristic MT "kink" at the surface interface. However, the rotational mobility of this "kink" (wobbling mode) which is integral to our theory will be affected in a slightly different manner.

If in case S1, in the adsorbed section, the polymorphic order parameter P can rearrange to some extent (by switching the monomer states without causing detectable deformation) except for possibly in the few surface-interacting dimers, then the effects of the "wobbling" motion will be hindered only mildly in the following sense. To retrieve the anomalous lateral fluctuations it is indeed enough for the wobbling angle ϕ_0 to move freely in a certain nonvanishing angular interval. A single complete or multiple rotations of the order parameter $\vec{P}$ are not strictly necessary for the "hinge" effect, and they are in fact equivalent in lateral projection (as in experiment) to the motion of the wobbling angle ϕ_0 in the smaller interval $[-\pi/2, +\pi/2]$. Note that even intervals smaller than this will lead to a similar phenomenology (in particular, dynamic and static
variable scalings with length). Thus, the conical hinge-like motion is in a sense robust with respect to a limited local rotational hindrance perturbation in the adsorbed region.

In scenario S2 the situation is somehow simpler as the polymorphic dynamics of the adsorbed region is not involved in the process (the polymorphic order parameter vanishes there: $\vec{P} = 0$). Wobbling is realized through a coherent rearrangement of the free MT section alone, without strong coupling to the adsorbed region.

Although both attachment scenarios S1 and S2 appear to some extent plausible, at present it is difficult to make reliable statements about their respective likelihood. In fact only a posteriori can we cautiously state that, based on the experimental static and dynamic measurement evidence, the chain "wobbles" to a high enough extent to display the effects that we observe.

References

Alberts B, Johnson A, Lewis J, Raff M, Roberts K, Walter P (2002) Molecular biology of the cell, 4th edn. Garland Science, New York

Amos LA (1991) Negative Stain electron microscopy of microtubules and associated motor molecules. Micron Microsc Acta 22:395

Amos LA, Amos WG (1991) Molecules of the cytoskeleton. Guilford, New York

Amos LA, Amos WB (1991) The bending of sliding microtubules imaged by confocal light microscopy and negative stain electron microscopy. J Cell Sci Suppl 14:95–101

Amos LA, Löwe J (1999) How taxol stabilises microtubule structure. Chem Biol 6:R65–R69

Arnal I, Wade RH (1995) How does taxol stabilize microtubules?. Curr Biol 5:900–908

Asakura S (1970) Polymerization of flagellin and polymorphism of flagella. Adv Biophys (Japan) 1:99–155

Bicek AD, Tüzel E, Demtchouk A, Uppalapati M, Hancock WO, Kroll DM, Odde DJ (2009) Anterograde microtubule transport drives microtubule bending in LLC-PK1 epithelial cells. Mol Biol Cell 20:2943

Bouchet-Marquis C, Zuber B, Glynn A-M, Eltsov M, Grabenbauer M, Goldie KN, Thomas D, Frangakis AS, Dubochet J, Chrétien D (2007) Visualization of cell microtubules in their native state. Biol Cell 99:45–53

Brangwynne CP, MacKintosh FC, Kumar S, Geisse NA, Talbot J, Mahadevan L, Parker KK, Ingber DE, Weitz DA (2006) Microtubules can bear enhanced compressive loads in living cells because of lateral reinforcement. J Cell Biol 173:733–741

Brangwynne C, Koenderink G, Barry E, Dogic Z, MacKintosh F, Weitz D (2007) Bending dynamics of fluctuating biopolymers probed by automated high-resolution filament tracking. Biophys J 93:346–359

Calladine CR (1975) Construction of bacterial flagella. Nature (London) 255:121–124

Chretien D, Fuller SD (2000) Microtubules switch occasionally into unfavorable configurations during elongation. J Mol Biol 298:663–676

Chretien D, Wade RH (1991) New data on the microtubule surface lattice. Biol Cell 71:161–174

Chrétien D, Metoz F, Verde F, Karsenti E, Wade RH (1992) Lattice defects in microtubules: protofilament numbers vary within individual microtubules. J Cell Biol 117:1031–1040

Chrétien D, Flyvbjerg H, Fuller SD (1998) Limited flexibility of the inter-protofilament bonds in microtubules assembled from pure tubulin. Eur Biophys J 27:490–500

Davis LJ, Odde DJ, Block SM, Gross SP (2002) The importance of lattice defects in Katanin-mediated microtubule severing in vitro. Biophys J 82:2916

Desai A, Verma S, Mitchison TJ, Walczak CE (1999) Kin I kinesins are microtubule-destabilizing enzymes. Cell 96:69–78

Elie-Caille C, Severin F, Helenius J, Howard J, Muller DJ, Hyman AA (2007) Straight GDP–tubulin protofilaments form in the presence of taxol. Curr Biol 17:1765–1770

Erickson HP, O'Brien ET (1992) Microtubule dynamic instability and GTP hydrolysis. Annu Rev Biophys Biomol Struct 21:145–166

Felgner H, Frank R, Schliwa M (1996) Flexural rigidity of microtubules measured with the use of optical tweezers. J Cell Sci 109:509–516

Fridoon JA, Hughey J, Wittmann T, Hyman A, Greaser M, Baas PW (2000) Motor proteins regulate force interactions between microtubules and microfilaments in the axon. Nature Cell Biol 2:276

Gittes F, Mickey B, Nettleton J, Howard J (1993) Flexural rigidity of microtubules and actin filaments measured from thermal fluctuations in shape. J Cell Biol 120:923–934

Hartman JJ, Mahr J, McNally K, Okawa K, Iwamatsu A, Thomas S, Cheesman S, Heuser J, Vale RD, McNally FJ (1998) Katanin, a microtubule-severing protein is a novel AAA ATPase that targets to the centrosome using a WD40-containing subunit. Cell 93:277–287

Heussinger C, Bathe M, Frey E (2007) Statistical mechanics of semiflexible bundles of wormlike polymer chains. Phys Rev Lett 99:048101

Howard J (2001) Mechanics of motor proteins and the cytoskeleton. Sinauer, Sunderland

Huilin J, De Rosier DJ, Nicholson WV, Nogales E, Downing KH (2002) Microtubule structure at 8 Å resolution. Structure 10:1317–1328

Hunyadi V, Janosi IM (2007) Metastability of microtubules induced by competing internal forces. Biophys J 92:3092–3097

Janosi IM, Chretien D, Flyvbjerg H (2002) Structural microtubule cap: stability, catastrophe, rescue, and third state. Biophys J 83:1317–1330

Janson ME, Dogterom M (2004) A bending mode analysis for growing microtubules: evidence for a velocity-dependent rigidity. Biophys J 87:2723–2736

Kaech S, Ludin B, Matus A (1996) Cytoskeletal plasticity in cells expressing neuronal microtubule-associated proteins. Neuron 17: 1189

Keating TJ, Peloquin JG, Rodionov VI, Momcilovic D, Borisy GG (1997) Microtubule release from the centrosome. Proc Natl Acad Sci USA 94:5078

Keller PJ, Pampaloni F, Lattanzi G, Stelzer EHK (2008) Three-dimensional microtubule behavior in Xenopus egg extracts reveals four dynamic states and state-dependent elastic properties. Biophys J 95:1474

Kikumoto M, Kurachi M, Tosa V, Tashiro H (2006) Flexural rigidity of individual microtubules measured by a buckling force with optical traps. Biophys J 90:1687–1696

Kim T, Kao MT, Hasselbrink EF, Meyhöfer E (2008) Nanomechanical model of microtubule translocation in the presence of electric fields. Biophys J 94:3880–3892

Kis A, Kasas S, Babic B, Kulik AJ, Benoit W, Briggs GA, Schonenberger C, Catsicas S, Forro L (2002) Nanomechanics of microtubules. Phys Rev Lett 89:248101

Kol N, Adler-Abramovich L, Barlam D, Shneck RZ, Gazit E, Rousso I (2005) Self-assembled peptide nanotubes are uniquely rigid bioinspired supramolecular structures. Nano Lett 5:1343

Kulic IM, Brown AEX, Kim H, Kural C, Blehm B, Selvin PR (2008) The role of microtubule movement in bidirectional organelle transport. Proc Natl Acad Sci USA 105:10011–10016

Kurachi M, Hoshi M, Tashiro H (1995) Buckling of a single microtubule by optical trapping forces: direct measurement of microtubule rigidity. Cell Motil Cytoskeleton 30:221–228

Löwel J, Li H, Downing KH, Nogales E (2001) Refined structure of $\alpha\beta$-Tubulin at 3.5 Å resolution. J Mol Biol 313:10451–10457

Mandelkow EM, Mandelkow E, Milligan RA (1991) Microtubules dynamics and microtubules caps: a time-resolved cryoelectron microscopy study. J Cell Biol 114:977–991

Mickey B, Howard J (1995) Rigidity of microtubules is increased by stabilizing agents. J Cell Biol 130:909–917

Mitchison T, Kirschner MW (1984) Dynamic instability of microtubule growth. Nature 312:237–242

Mohrbach H, Kulic IM (2007) Motor driven microtubule shape fluctuations: force from within the lattice. Phys Rev Lett 99: 218102

Mohrbach H, Johner A, Kulic IM (2010) Tubulin bistability and polymorphic dynamics of microtubules. Phys Rev Lett 105: 268102

Muto E, Sakai H, Kaseda K (2005) Long-range cooperative binding of kinesin to a microtubule in the presence of ATP. J Cell Biol 168:691

Nogales E, Wolf SG, Downing KH (1998) Structure of the $\alpha\beta$ tubulin dimer by electron crystallography. Nature 391:199–203

Nogales E, Whittaker M, Milligan RA, Downing KH (1999) High resolution model of the microtubule. Cell 96:79–88

Nogales E, Wang HW, Niederstrasser H (2003) Tubulin rings: which way do they curve ?. Curr Opin Struct Biol 13:256–261

Pampaloni F, Lattanzi G, Jonas A, Surrey T, Frey E, Florin EL (2006) Thermal fluctuations of grafted microtubules provide evidence of a length-dependent persistence length. Proc Natl Acad USA 103:10248–10253

Ray S, Meyhofer E, Milligan RA, Howard J (1993) Kinesin follows the microtubule's protofilament axis. J Cell Biol 121:1083–1093

Samsonov A, Yu J-Z, Rasenick M, Popov SV (2004) Tau interaction with microtubules in vivo. J Cell Sci 117:6129

Takasone T, Juodkazis S, Kawagishi Y, Yamaguchi A, Matsuo S, Sakakibara H, Nakayama H, Misawa H (2002) Flexural rigidity of a single microtubule. Jpn J Appl Phys 41:3015–3019

Taute KM, Pampaloni F, Frey E, Florin E-L (2008) Microtubule dynamics depart from the wormlike chain model. Phys Rev Lett 100:028102

Vale RD, Coppin CM, Malik F, Kull FJ, Milligan RD (1994) Tubulin GTP hydrolysis influences the structure, mechanical properties and kinesin-driven transport of microtubules. J Biol Chem 269: 23769–23775

Vanden Heuvel MGL, Bolhuis S, Dekker C (2007) Persistence length measurements from stochastic single-microtubule trajectories. Nano Lett 7:3138

Vanden Heuvel MGL, de Graaff MP, Lemay SG, Dekker C (2007) Electrophoresis of individual microtubules in microchannels. Proc Natl Acad Sci USA 104:7770–7775

Vanden Heuvel MGL, de Graaff MP, Dekker C (2008) Microtubule curvatures under perpendicular electric forces reveal a low persistence length. Proc Natl Acad Sci USA 105:7941

Venier P, Maggs AC, Carlier MF, Pantaloni D (1994) Analysis of microtubule rigidity using hydrodynamic flow and thermal fluctuations. J Biol Chem 269:13353

Wade RH, Chrétien D, Job D (1990) Characterization of microtubule protofilament numbers. How does the surface lattice accommodate?. J Mol Biol 212:775–786

Xiao H, Verdier-Pinard P, Fernandez-Fuentes N, Burd B, Angeletti R, Fiser A, Horwitz SB, Orr GA (2006) Insights into the mechanism of microtubule stabilization by taxol. Proc Natl Acad Sci USA 103:10166–10173